ACKNOWLEDGMENT

I would like to express a deep gratitude to my advisor Professor Scott T. Dunham, for his guidance and encouragement throughout the entirety of my study at Boston University and this graduate research work on the VLSI fabrication process modeling. I would like to express sincere appreciation to Professor Yaneer Bar-Yam, for his help and guidance to start my study at Boston University and my graduate research on GWA techniques for *ab initio* total-energy calculations. Also, I would like to thank Professor Selim Unlu for providing a very timely reading of this manuscript and valuable suggestions.

A great deal of thanks go to my office-mates and friends, Fred Wittel, Anu Agarwal, Iuval Clejan, Mitra Navi and Misako Matsuoka, for their beneficial advice, enlightening discussions and warm companionship made my days at Boston University a cherished memory. I owe Fred Wittel a big thanks for helping me not only to understand and solve the problems on VLSI fabrication process modeling, but also to learn a lot about the American cultures and values.

Finally, a special thank is sent to my wife Jinjin Gu. Her love and support are the greatest resources of motivation and inspiration in my life.

Monte Carlo Lattice Simulations of Vacancy-Mediated Diffusion in Silicon

(Order No.)

Can-Dong Wu
Boston University, College of Engineering, 1994
Major Professor: Scott T. Dunham, Professor of Electrical Engineering.

Abstract

To investigate vacancy-mediated diffusion of dopant atoms in silicon, diffusion models based on atomistic analysis are proposed and Monte-Carlo random walk simulations of hopping diffusion are implemented on a three dimensional diamond lattice structure. The dopant atom and vacancy interaction potentials are assumed to extend out to third-nearest neighbor distances. The dopant-vacancy pair binding energies correspond to the silicon materials doped by arsenic at 915°C and 1050°C and phosphorus at 1050°C. With a fixed free vacancy concentration, the Monte-Carlo simulations trace vacancy motion and verify the atomistic diffusion model for moderately doped materials. For very high doping density ($> 2 \times 10^{20}\text{cm}^{-3}$), the simulations show a very rapid increase in dopant diffusivity due to interactions of vacancies with more than one dopant atom. This behavior has been observed experimentally for group IV and V atoms in silicon [Nylandsted Larsen *et al., J. Appl. Phys.* **73**, 691 (1993)]. The simulations predict both the point of onset and doping dependence of the experimentally-observed diffusivity enhancement. Further simulations also examine the dopant flux caused by a vacancy gradient, leading to a modification of the continuity equation for vacancy pair diffusion.

Contents

Chapter 1

Introduction

It has become accepted that the diffusion of dopant atoms in the silicon lattice takes place via interactions with vacancies and interstitials [1]. There are many papers reporting on this subject [2, 3, 4, 5]. However, dopant atom/point defect coupled diffusion is a complex process and remains incompletely understood. Traditional physical measurements and empirical analysis are unable to offer a clear view into all the details of point defect mediated dopant diffusion. An accurate model is desirable, especially for the fabrication processes of small dimensional VLSI devices.

Vacancies and intersitials are two important types of the point-defects involved in the diffusion process. This research will focus on the vacancy and concentrate on the interactions between dopant atoms and vacancies only. In particular, we investigate how doping density or dopant-vacancy pair density affects the dopant diffusivity in silicon both at moderate doping levels and at very heavy doping levels.

Previous research [6] has noted that the third-nearest neighbor dopant-vacancy pair is crucial to the coupled diffusion process, but the implications of this central role have not been completely explored. It is still a question how the binding energies of dopant-vacancy pairs with different neighboring distances (i.e. of the 1st-nearest neighbor sites ΔE_1, of the 2nd-nearest neighbor sites ΔE_2, and of the 3rd-nearest neighbor sites ΔE_3), will affect the values of diffusivity. There are also contentious arguments over the role of dopant-vacancy interaction in the diffusion process at heavily-doped materials [4, 7, 8, 9, 10, 11, 12]. Another interesting issue is raised about whether a vacancy gradient will result in a dopant flux in the same or opposite direction as the vacancy flux has [13, 14, 15].

Despite its appreciable computational cost, the simplicity of implementation and the relatively complete description of microscopic transport phenomena have rendered Monte Carlo (MC) simulation appealing to research on the topic of dopant-vacancy paired diffusion. Based on the atomistic analysis, this work takes advantage of the merits of MC simulation to trace the particles (dopants, vacancies and silicon atoms), and by observing the motions and interactions of dopants and vacancies throughout the complex microcosmos of diffusion, to find out answers fundamental to understanding diffusion processes in silicon.

Focusing on the vacancy mediated diffusion in silicon lattice structure, this thesis will present the important theoretical analyses, the MC simulations and the discussions of the results. Chapter 2 includes a review of the vacancy diffusion mechanism and pair diffusion models and Chapter 3 introduces the atomistic model, which becomes a guideline to the MC simulations and the analyses of computational results. Chapter 4 describes the implementation of MC lattice simulations with a C-language program. Based on the results from MC simulations and the comparison to the atomistic model predictions, Chapter 5 explores the diffusivity as a function of dopant density and the diffusion behavior in heavily-doped materials. Chapter 6 develops the MC simulations for the dopant diffusion caused by a vacancy gradient. Finally, Chapter 7 contains the conclusions of this research and suggestions for the future work.

Chapter 2

Background and the Vacancy Mechanism

After the pioneering works done by Hu *et al.* [2, 16], most diffusion models have evolved to support the idea that dopants diffuse primarily by vacancy and/or interstitial mechanism. For the diffusion process occurring at high temperature ($T > 900^{o}$C), both vacancies and interstitials have crucial interactions with the dopant atoms [1]. However, this work only considers vacancies. We need a suitable model of vacancy-mediated dopant diffusion as a guideline to the Monte-Carlo simulations and thus, a brief review of the vacancy mechanism becomes an indispensable part of the thesis.

2.1 The Dopant/Vacancy Site-Exchange

Based on vacancy mechanism [1], the dopant diffusion can be visualized as a kinetic process by which the dopant atoms exchange the lattice sites with their adjacent vacancies. Therefore, the vacancy becomes the medium of diffusion. The vacancy could exchange the lattice site with a dopant atom, a silicon atom or another vacancy. However, in order to have a long range dopant migration, a special requirement should be met by the motion of vacancy.

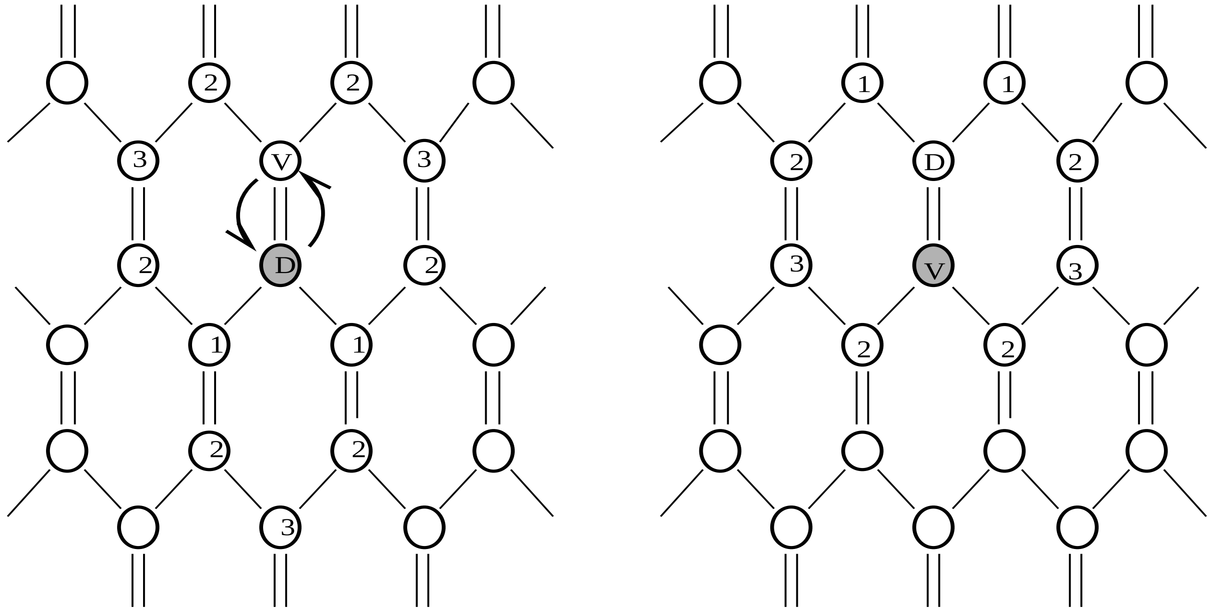

(a) (b)

Figure 2.1: Dopant site with vacancy neighbor in the silicon lattice structure as viewed in $\langle 110 \rangle$ direction with a shaded original site: (a) an arrow pair indicates a possible dopant-vacancy site exchange; (b) the neighborhood after the site exchange of (a). The number indicates the ith nearest-neighbor site of dopant.

The following is an example of how a vacancy enables the dopant to complete one step of long range migration. Figure 2.1(a) and 2.1(b) show a $\langle 110 \rangle$ direction view into the three-dimensional diamond lattice structure. Assuming that before the dopant-vacancy site exchange, a dopant atom (marked as "D") sits at the shaded original site and a vacancy sits at one of the first-nearest neighbor sites (marked as "V") in Figure 2.1(a), we can imagine a possible site-exchange occurring to the dopant and the vacancy, marked by a pair of arrows in Figure 2.1(a).

Figure 2.1(b) shows the case after the site-exchange of Figure 2.1(a). The vacancy now sits at the shaded original site. The next site-exchange after Figure 2.1(b) would put dopant back to the shaded site again by the reverse of the previous site-exchange of Figure 2.1(a). If such a forward-backward loop continues, the dopant would still sit on the original site shaded in Figure 2.1 after any even numbers of site-exchanges counted from the beginning of Figure 2.1(a). Thus, if the vacancy is always sitting at one of the adjacent sites to the dopant, long range dopant diffusion can never take place.

To make long-range dopant migration possible, the vacancy must keep hopping, via sites marked as “2” in Figure 2.1(b) to one of the third-nearest neighbor sites (marked as “3”). Then, the vacancy can jump via a different site “2” to the site marked as “1” in Figure 2.1(b). Once it is at site “1” in Figure 2.1(b), the vacancy will be likely have a site-exchange with the dopant at site marked as “D” in Figure 2.1(b) and enable dopant to migrate to a new site, which is no longer adjacent to the shaded site in Figure 2.1(a).

As a conclusion, after the original site-exchange with the dopant, a vacancy must move away to at least a third-nearest neighbor distance from the dopant, then it is possible for the vacancy to have a site-exchange with the dopant along a different path and to complete one step of dopant diffusion in the diamond lattice. This process must occur over and over to continue the long range migration of the dopant atom.

2.2 The Dopant-Vacancy Pair Diffusion

As stated earlier, this research focuses on the dopant-vacancy pair interactions and does not consider the interstitial interactions with the dopant atoms. The standard model for dopant diffusion in silicon assumes that dopants and defects form pairs that move together through the lattice [1]. Based on the pair diffusion model, the dopant flux due to vacancies is given by:

$$J_D \quad = \quad -D_{DV} \nabla C_{DV}, \qquad (2.1)$$

where C_{DV} is the dopant-vacancy pair concentration and D_{DV} is the pair diffusivity. The mass-action relation between the dopant, vacancy and dopant-vacancy pair is given by

$$D + V \quad \Longleftrightarrow \quad DV. \qquad (2.2)$$

In equilibrium, the forward and reverse rates are equal to each other, i.e.

$$\begin{aligned} k_f C_D C_V &= k_r C_{DV} \\ C_{DV} &= \frac{k_f}{k_r} C_D C_V. \end{aligned} \tag{2.3}$$

where k_f/k_r depends only on the temperature.

Now we should discuss the activation energies involved in the diffusion process

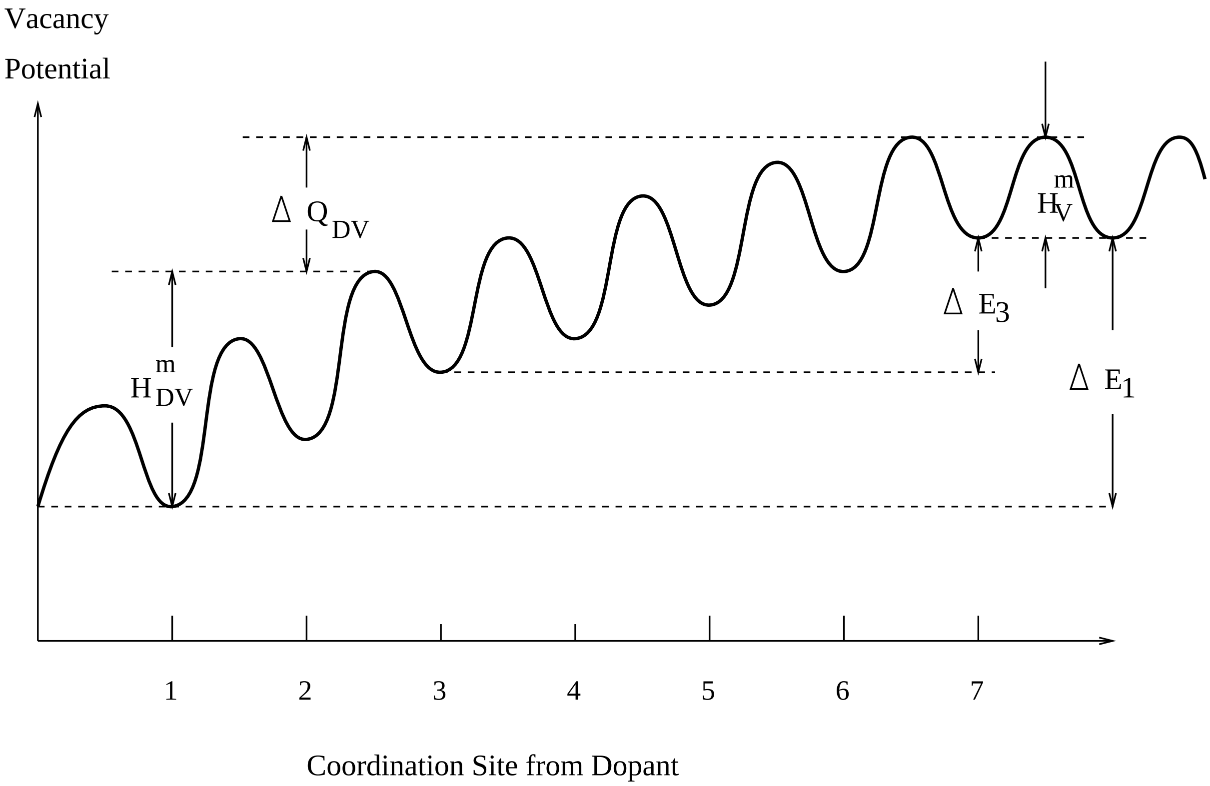

Figure 2.2: Vacancy Potential as a function of coordination site away from a dopant atom.

based on Hu's analysis of pair diffusion [1, 17]. To analyze the energetics of diffusion, we take the self diffusion as an energy reference in the system and define the following quantities:

$$Q_{SiV} - Q_{DV} = \Delta Q_{DV} \tag{2.4}$$

where Q is the label for activation energy and ΔQ_{DV} is the difference in activation energy between the self- and dopant diffusion that proceed by the vacancy mechanism. The activation energies can be written as

$$Q_{SiV} = H_V^m + H_V^f \tag{2.5}$$

$$Q_{DV} = H_{DV}^m + H_{DV}^f, \tag{2.6}$$

where H_V^m and H_V^f are the migration and the formation enthalpies of an unpaired vacancy, and H_{DV}^m and H_{DV}^f are of dopant-vacancy pair.

As indicated in Figure 2.1, ΔE_1 is defined as the binding energy between the dopant atom and the vacancy at the first-nearest neighbor sites, and ΔE_3 is defined as the binding energy between the dopant atom and the vacancy at the third-nearest neighbor sites. Hu [17] asserted the relationship of

$$\begin{aligned} H_{DV}^f &= H_V^f - \Delta E_1 \\ H_{DV}^m &= H_V^m + \Delta E_1 - \Delta E_3. \end{aligned} \tag{2.7}$$

With Eq. (2.5) to Eq. (2.7), it is easy to derive that

$$Q_{SiV} - Q_{DV} = \Delta Q_{DV} = \Delta E_3. \tag{2.8}$$

Eq. (2.8) means that by the vacancy mechanism, the activation energy of dopant diffusion is an amount ΔE_3 lower than the corresponding activation energy of self-diffusion.

The reason for only the term ΔE_3 appearing in Eq. (2.8) is that Hu assumed that the vacancy has the same migration energy anywhere in the system. However, this assumption is contrary to the curve of Figure 2.1 used by Hu [17]. From Figure 2.2, we find that for a vacancy existing within the interaction range of a dopant atom, the potential barrier for vacancy migration varies from site to site. To describe the interaction potentials and migration energy barriers with different pairing distances, we need a new atomistic model which will be discussed in Chapter 3.

2.3 Fermi-level Charge State Effects

The diffusion of group V impurities in silicon has been discussed within a model which considers Fermi-level-dependent point-defect concentrations [1, 18]. Taking the negatively charged vacancy V^- as an example, the vacancy concentration depends on the Fermi-level effect in the following way [19]

$$C_V^- = C_V^0 \left(\frac{n}{n_i}\right) \exp\left(\frac{E_V - E_i}{kT}\right), \tag{2.9}$$

where E_i is the intrinsic Fermi level and E_{V^-} is the energy level of the negatively charged vacancy. If the vacancies have different charge states [20], the effective diffusivity of vacancy-assisted dopant diffusion is

$$D_{\text{eff}} = D^0 + D^- \left(\frac{n}{n_i}\right) + D^= \left(\frac{n}{n_i}\right)^2, \tag{2.10}$$

where, n_i and n are the intrinsic and actual electron concentrations respectively, D^0 is the dopant diffusivity dependent on the vacancy in the neutral charge state, and the terms of D^- and $D^=$ represent the coefficients of diffusion mediated by singly- and doubly- negative charged vacancies.

From the experimental data of arsenic doping diffusion, Fair *et al.* [18] proposed the diffusivity of arsenic as

$$D_{As} = D^0 + D^- \left(\frac{n}{n_i}\right). \tag{2.11}$$

Based on phosphorus diffusion in n-type materials, Wittel and Dunham [27] also found that the dopant diffusivity never varies more strongly than linearly with the carrier concentration and the $D^=$ term is not necessary to include in Fermi-level effects. Further, in n-type materials diffusion with negatively-charged vacancies become dominant. Therefore, to simplify the analysis, we will focus on a single charge state of dopant atoms and vacancies. The Fermi-level effects for donors in moderately to heavily doped materials can be expressed as

$$D_{\text{eff}} \simeq D^- \left(\frac{n}{n_i}\right). \tag{2.12}$$

Nylandsted Larsen *et al.* [10, 28, 29] observed that when the doping density of arsenic, antimony, tin or germanium in silicon is above $2 \times 10^{20}\text{cm}^{-3}$, the dopant diffusivity increases in proportion to the third to fifth power of the doping density.

Since a dopant diffusion via triple- or penta-charged vacancies is not expected to be significant, Larsen *et al.* pointed out that for very heavy doping diffusion, the Fermi-level charge state model of Eq. (2.10) is no longer adequate. The heavy doping density diffusion was considered as a percolation problem by Mathiot *et al.* [7, 10]. In Chapter 5, we will discuss and comment on the percolation model.

Chapter 3

Atomistic Model of Vacancy-Mediated Diffusion

Due to the dopant-vacancy binding energies, more vacancies can be expected in the vicinity of the dopant atoms than in remote areas where no dopant atom exists. Such a phenomenons was explained as a reduction in the quasi-vacancy formation energy in the work of Yoshida [3]. In order to distinguish the vacancies in two areas, we call the vacancies at the undoped area (beyond the interaction distance from any dopant) as free vacancies, and the vacancies associated with dopant atoms as paired vacancies.

This chapter will introduce the atomistic model proposed by this research. This new model describes how dopant-vacancy neighboring distances affect the binding energies. The atomistic model can accurately formulate the diffusivity as a function of the binding energies for moderately doped materials. Moreover, it is able to deal with the heavy doping behavior by which the dopant diffusivity depends not only on the binding energies but also on the doping density.

3.1 Hopping Diffusion

In the review of the vacancy mechanism in Chapter 2, the dopant-vacancy site-exchange is described as an accepted mechanism for dopant diffusion through the silicon lattice. If the diffusion process is carried out by atom's jumping from one lattice site to another, it can be characterized as hopping diffusion. For hopping diffusion in a three-dimensional lattice structure, the diffusivity can be expressed as [32]:

$$D = \frac{1}{6}\alpha^2 \nu_{\text{eff}} \tag{3.1}$$

where, $\alpha = \sqrt{3}a/4$ is the single jump distance with lattice constant a (for silicon lattice, $a = 5.43\text{Å}$) and ν_{eff} is the effective mean hopping rate.

The collective result of ν_{eff} is contributed from the statistical summation of all individual hops. If atom hops are correlated with previous hopping steps, the effective mean hopping rate is expressed as

$$\nu_{\text{eff}} = f \sum \nu_j \tag{3.2}$$

where f is the correlation factor and ν_j is the rate of jth possible hop configuration.

3.1.1 Self-Diffusion Coefficient

By using vacancy mechanism and hopping diffusion model, we are able to derive the coefficient of self-diffusion. For tracer self-diffusion via vacancies through the diamond lattice, a previous calculation indicated that the correlation factor is given by $f = 0.5$ [21]. In addition, each atom should have the same hop rate to its four adjacent sites. Thus,

$$\sum \nu_j = 4 \times \nu_V^0 \left(\frac{C_V^0}{C_S}\right) \tag{3.3}$$

where ν_V^0 is the hopping rate of free vacancy, C_V^0 is the free vacancy concentration, and C_S is the concentration of lattice sites. Therefore, using Eq. (3.1) and Eq. (3.3), we have the coefficient of tracer self-diffusion via vacancies as

$$D_{\text{self}} = \frac{a^2\nu_V^0}{16}\left(\frac{C_V^0}{C_S}\right), \tag{3.4}$$

where (C_V^0/C_S) is the fraction of lattice sites occupied by vacancies.

3.1.2 Hopping Diffusion Model for Dopants

In the doped region, there is a larger vacancy concentration due to the dopant-vacancy binding energies. However, the effective hopping rate of the dopant is much lower than the rate of dopant displacement, since the dopant/vacancy site-exchange could simply restore the dopant to its original site after two site-exchange steps and such a forward-backward loop could repeat itself many times. As described in Section 2.1, the vacancies at the third-nearest neighbor sites are critical to dopant diffusion, since they offer possible routines for dopants to move away from one site to another with a relatively long range of migration. Thus, the effective hopping rate ν_{eff} is related to the rate of hopping from the second to the third nearest neighbor ($3nn$) site combined with the concentration of $3nn$ dopant/vacancy pairs C_{DV}^{3nn} [22, 23]. The effective hopping rate can be formulated as:

$$\nu_{\text{eff}} = f\nu_{32}\left(\frac{C_{DV}^{3nn}}{C_D}\right) \tag{3.5}$$

where ν_{32} is the rate of a single vacancy hopping from the third- to the second-nearest neighbor site. To complete one step of long range dopant migration, the vacancy must move away to at least the $3nn$ site after the original site-exchange with the dopant atom. Thus, the pair must partially dissociate and reform many times.

The correlation factor f in Eq. (2.6) is given by [24]:

$$f = \frac{1+\langle\cos\theta\rangle}{1-\langle\cos\theta\rangle} \tag{3.6}$$

The $\langle\cos\theta\rangle$ in Eq. (2.7) represents the average value of displacement projection of two consecutive hopping steps. There are two possible patterns for the atom at each third-nearest neighbor site within the diamond lattice structure. One is just a reversal of the previous hop with $\cos\theta = -1$, while the other is a forward hop along the diamond bonding chain with $\cos\theta = 1/3 \quad (\theta = 70.6^o)$. Then, we have $\langle\cos\theta\rangle = (-1+1/3)/2 = -1/3$ and $f = 0.5$.

From the hopping diffusion model, the dopant diffusivity is given by

$$D_D = \frac{\alpha^2\nu_{32}}{12}\left(\frac{C_{DV}^{3nn}}{C_D}\right). \tag{3.7}$$

In order to specify the dopant diffusivity, we need the expressions for the hopping rate ν_{32} and pair concentration C_{DV}^{3nn} in terms of the binding energies and the coefficient of self-diffusion. We will start by considering moderately doped materials before considering effects which occur in very heavily doped materials.

3.2 Diffusion in Moderately-Doped Materials

In this section, by saying "moderately doped materials", we mean that the doping density C_D is lower than $10^{20}\mathrm{cm}^{-3}$ so that in the lattice structure, almost all dopant atoms are separated by at least the distance of the sixth-nearest neighbor site away from each other by silicon atoms and/or vacancies. The reason of our definition will be emphasized later.

3.2.1 The Binding Energies of Dopant-Vacancy Pair

As explained in Chapter 2, this research assumes that the dopant migration happens only when a dopant atom exchanges the site with a vacancy which is at one of four adjacent sites. The change for total binding energies in the system becomes the driving force of pair motions. In order to avoid an endless loop of backward and forward dopant-vacancy site exchange, there must be some long-range vacancy-dopant binding energies to enhance the rate of long range migration.

There are always some interaction potentials between a dopant atom and its neighboring vacancy with the first-, the second-, the third-, the fourth-nearest neighbor distance and so on. An ideal model should include as many of these interaction terms as possible. In order to make the simulation program less complicated, we consider only the pair binding energies to the 3rd-nearest neighbor distance to meet the requirement of the vacancy mechanism. Therefore, in this research, there are only three types of dopant-vacancy pairs, i.e. the pairs with the first-nearest neighbor ($1nn$), the second-nearest neighbor ($2nn$) or the third–nearest neighbor ($3nn$) site distance. Any vacancies at the sites farther than the $3nn$ sites are considered as free vacancies. Represented in units of lattice constant a of the diamond cubic cell, the distance of the $1nn$ site is $0.433013a$, the $2nn$ site is $0.707107a$ and the $3nn$ site is $0.829156a$.

Figure 3.1 indicates the binding energy as a function of the distance between

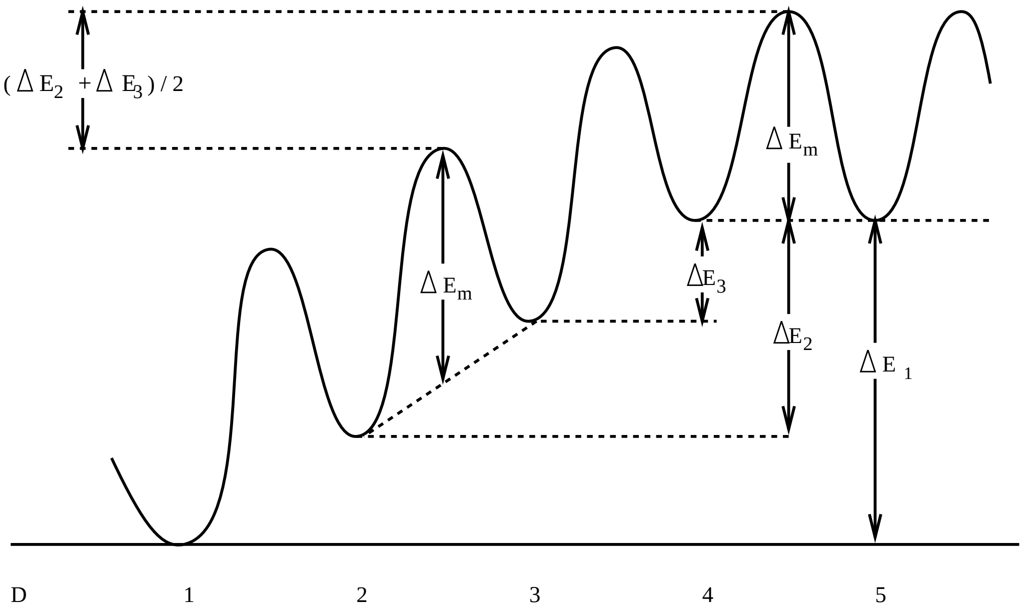

Figure 3.1: Schematic of vacancy-dopant binding energy as a function of neighboring site positions for a dopant atom in moderately-doped materials.

dopant and vacancy sites. The positions of the atom sites are indicated in Figure 3.1, where D is the site of dopant atom, and 1, 2, ..., n are the nth nearest neighbor sites. The binding energies at the first, second and third-nearest neighbor distance ($\Delta E_1, \Delta E_2$, and ΔE_3), are equal to the energies required for moving a vacancy away from ith neighbor site to the remote area. During the migration, the vacancy is in a stable energy states when it sits at one of the site positions in Figure 3.1 and becomes unstable at the peak points while it is overcoming the energy barrier for migration.

For the energy curve of Figure 3.1, ΔE_m is the vacancy migration energy in the remote area with $3nn$ site distance away from any dopant atom. Within the range of $3nn$ site distance, the energy barrier is equal to ΔE_m plus half the potential difference between the initial and final vacancy site.

As an application of Figure 3.1, the rate for a vacancy migrating from the ith site to the jth site ν_{ij} can be formulated as

$$\nu_{ij} \quad = \quad \nu_V^0 \exp\left(\frac{\Delta E_j - \Delta E_i}{2kT}\right). \tag{3.8}$$

where ν_V^0 is the hopping rate of the free vacancy. Thus, the binding energy difference determines the rate of a vacancy hopping from the $3nn$ site to the $2nn$ site as

$$\nu_{32} \quad = \quad \nu_V^o \exp(\frac{\Delta E_2 - \Delta E_3}{2kT}). \tag{3.9}$$

3.2.2 Diffusivity for Moderately-Doped Materials

Referring to the dopant-vacancy binding energy curve of Figure 3.1, we can set up a practical atomistic model for the diffusion process in the moderately-doped materials. All physical quantities needed to calculate the dopant diffusivity relative to the self-diffusion coefficient can be expressed as the functions of the dopant-vacancy binding energies.

With a constant free vacancy concentration C_V^0 in remote areas, the vacancy concentration in a doped region is decided by the dopant density and the binding energies. Dopant atom will attract vacancies to form dopant-vacancy pairs (i.e. $1nn$, $2nn$ and $3nn$ pairs) with the concentrations of

$$\frac{C_{DV}^{1nn}}{C_D} \quad = \quad 4(\frac{C_V^o}{C_S})\exp(\frac{\Delta E_1}{kT}), \tag{3.10}$$

$$\frac{C_{DV}^{2nn}}{C_D} \quad = \quad 12(\frac{C_V^o}{C_S})\exp(\frac{\Delta E_2}{kT}), \tag{3.11}$$

$$\frac{C_{DV}^{3nn}}{C_D} \quad = \quad 12(\frac{C_V^o}{C_S})\exp(\frac{\Delta E_3}{kT}). \tag{3.12}$$

where the factors 4 and 12 are number of the ith-nearest neighbor sites. The above expressions are based on a dilute solution and thus, the equation of C_{DV}^{3nn} is the best approximation among the three since ΔE_3 is the smallest binding energy.

Recalling Eq. (3.7) and Eq. (3.10), we get the expression for dopant diffusivity for the moderately doped materials as

$$D \quad = \quad \frac{\alpha^2}{12}[12\left(\frac{C_V^0}{C_S}\right)\exp\left(\frac{\Delta E_3}{kT}\right)][\nu_V^0 \exp\left(\frac{\Delta E_2 - \Delta E_3}{2kT}\right)]$$

$$= \frac{3a^2}{16}\left(\frac{C_V^0}{C_S}\right)\nu_V^0 \exp\left(\frac{\Delta E_2 + \Delta E_3}{2kT}\right), \tag{3.13}$$

where α is the hopping distance in the silicon lattice structure ($\alpha = \sqrt{3a}/4$ with the lattice constant $a = 5.43$Å). Normalized by the coefficient of self-diffusion D_{self} in Eq. (3.4), the dopant diffusivity can be written as

$$\frac{D}{D_{\text{self}}} = 3\exp\left(\frac{\Delta E_2 + \Delta E_3}{2kT}\right). \tag{3.14}$$

With Figure 3.1, the preexponential term in the diffusivity expression of Eq. (3.13) or Eq. (3.14) implies that the dopant diffusivity D is enhanced from the coefficient of self-diffusion D_{self} exponentially by the activation energy difference between the free vacancy and dopant/vacancy pair as

$$\Delta Q_{DV} = (\Delta E_2 + \Delta E_3)/2. \tag{3.15}$$

As shown in Figure 3.1, ΔQ_{DV} is equivalent to the total change of system energy after two stages (1) the vacancy migrates from the remote area to the $3nn$ site with $\Delta E^{(1)}_{\text{system}} = \Delta E_3$; (2) the forward and reverse process of vacancy hopping from the $2nn$ site to the $3nn$ site with $\Delta E^{(2)}_{\text{system}} = (\Delta E_2 - \Delta E_3)/2$ and finally, $\Delta E^{\text{total}}_{\text{system}} = \Delta E^{(1)}_{\text{system}} + \Delta E^{(2)}_{\text{system}}$. These two stages are both important to the dopant diffusion. In Hu's model [23], both stages were indicated by the energy curve in Figure 2.2, but only the first stage was counted for the activation energy difference as

$$\Delta Q_{DV} = Q_{SiV} - Q_{DV} = \Delta E_3. \tag{3.16}$$

Using a Coulombic potential, Hu calculated ΔQ_{DV} numerically, getting a value of $0.58\Delta E_1$ [17]. This value is much closer to the $0.57\Delta E_1$ calculated from our model than to the value of $0.52\Delta E_1$ from Hu's model. In the later chapters, we will find that the calculations from Eq. (3.14) are further validated by our Monte Carlo simulations.

3.3 Diffusion in Heavily-Doped Materials

The conclusion from Eq. (3.14) is that the normalized dopant diffusivity is independent of doping density for the moderately doped materials. One might ask what happens to the diffusivity if the doping density keeps increasing. Heavy-doping diffusion was investigated by Nylandsted Larsen *et al.* [10]. They observed the diffusion of As, Sb, Sn and Ge in the heavily phosphorus doped materials with typical results shown in Figure 3.2 [10]. We see that for moderate doping ($C_D < 10^{20}\mathrm{cm}^{-3}$), the diffusivity becomes $D_D \propto (C_D)$ due to diffusion via V^- ($C_{V^-} \propto n/n_i \propto C_D$). However for $C_D > 1.5 \times 10^{20}\mathrm{cm}^{-3}$, the diffusivity increases with a much stronger dependence on doping density $D_D \propto (C_D)^{(3\sim5)}$.

Heavily-doped materials are complicated systems involving different Fermi-level-

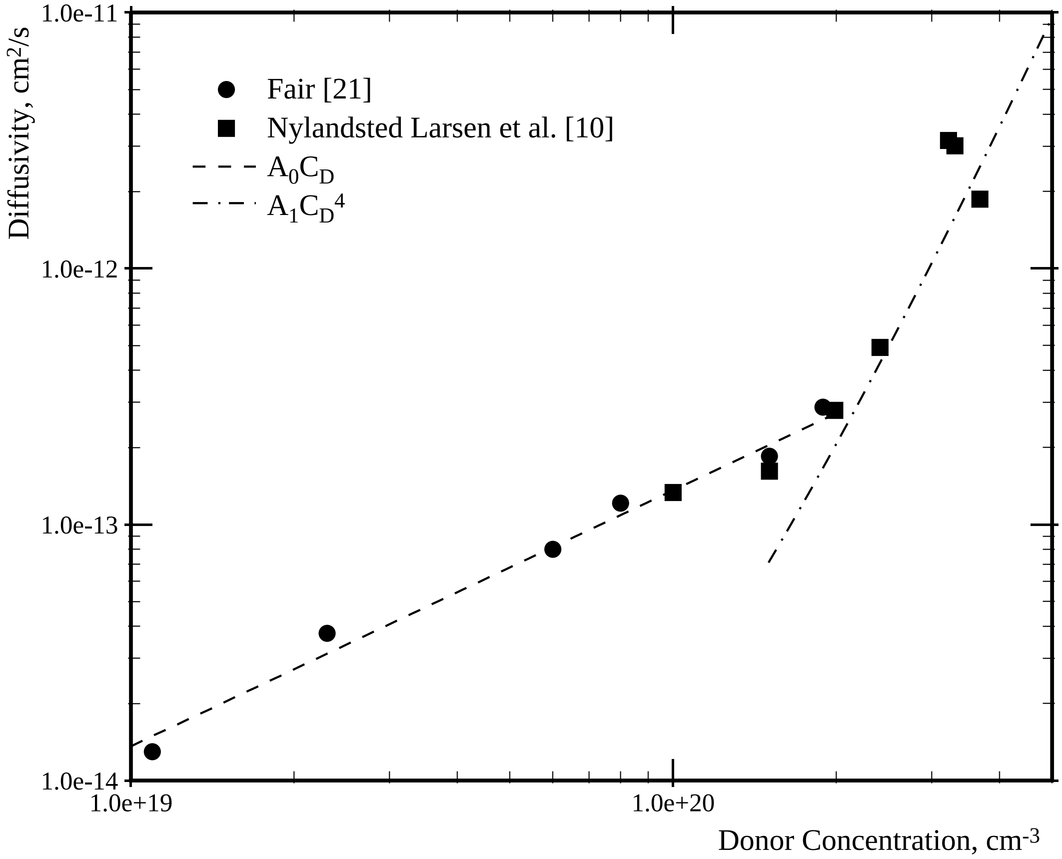

Figure 3.2: The experimental observations by Nylandsted Larsen *et al.* and Fair *et al.*, where the data are corresponding to the arsenic-diffusion coefficients at 1050^oC with different background doping densities. The dashed lines indicate the functions $D_D \propto C_D$ and $D_D \propto C_D^4$.

dependent charge states of the point defects, dopant-defect clustering and precipitation. In this research, we will show that collective dopant-vacancy pair effects play an important role.

3.3.1 The Collective Behavior of Dopant-Vacancy Pairs

For vacancy-assisted diffusion, in order to complete one step of dopant diffusion in silicon, the vacancy must diffuse to at least a $3nn$ distance away from the dopant atom so that it can return to a different adjacent site along a different path. For moderate doping diffusion, it is reasonable to believe that all dopant atoms are separated from each other by more than the distance to the sixth nearest neighbor site. Therefore, each vacancy is affected by the interaction with only one dopant atom at a time, and the dopant-vacancy pairs are isolated from each other.

As the doping density gets higher, the average distance among dopant atoms becomes shorter and the dopant-vacancy pair can no longer be considered as an isolated entity. In the heavily-doped region, a vacancy is likely to have interactions with more than one dopant atom at a time. This will result in an activation energy reduction for vacancy migration. A vacancy associated with two or more dopants, has lower energy to move from the $2nn$ sites to the $3nn$ sites than a vacancy in an isolated dopant-vacancy pair. The lower energy for transition state accelerates dopant diffusion by reducing the energy barrier of vacancy migration.

A special example of heavy-doping diffusion via vacancy mechanism is shown by Figure 3.3. The top-curve is the interaction potential for an isolated dopant-vacancy pair. After the doping density is increased, the upper curve is replaced by the bottom-curve, which represents the interaction potentials of a vacancy at different neighbor sites with two dopant atoms existing within the sixth-nearest neighbor distance.

Referring to the first dopant atom D_1 in Figure 3.3, if there is a second dopant atom D_2 on the sixth-nearest neighbor site, then site "3", is the third nearest neighbor for both dopant atoms D_1 and D_2. Comparing to the moderate-doping curve, the peak point between site "2" and site "3" of the heavy-doping curve has an interaction potential reduced by $\Delta E_3/2$. Therefore, the migration energy barrier for a vacancy

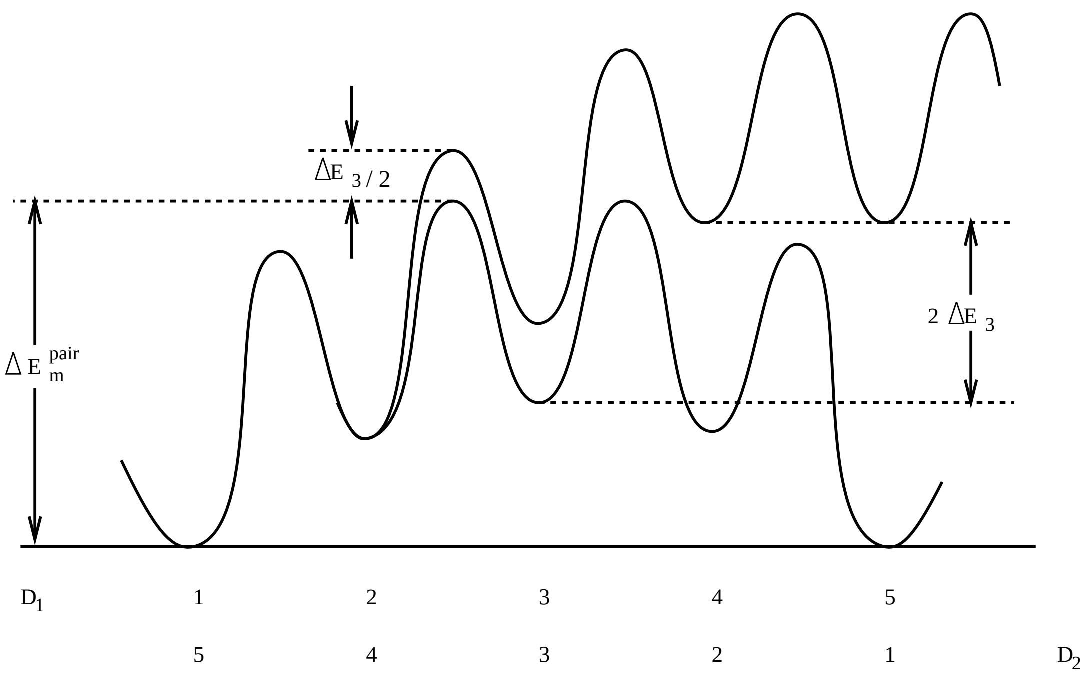

Figure 3.3: Comparison of vacancy-dopant binding energy as a function of neighborhood position of a dopant for normally- (top-curve) and heavily-doped (bottom-curve) materials.

hopping from site "2" to site "3" or from site "3" to site "2"is lowered by $\Delta E_3/2$. According to the vacancy mechanism introduced in Chapter 2, after an initial dopant-vacancy site exchange, the steps by which the vacancy migrates at least the $3nn$ site distance away from the dopant are very critical to long-range dopant diffusion. Now, because of the lower migration barriers in the heavily-doped systems, vacancies can more frequently complete these critical steps, and consequently the long-range dopant diffusion can be accelerated.

3.3.2 Heavy-Doping Diffusion Coefficient

As the doping density gets larger, the vacancy concentration C_V will be increased in the doped region because of associations with multiple dopant atoms. Based on the dilute solution approximation, we can get a formula for C_V.

For the first order approximation, the vacancy is paired by one dopant atom.

Thus the vacancy concentration depends on the doping density and all possible configurations having one vacancy at the neighboring sites of one dopant. Based on conditional probability calculation, the approximation is:

$$C_V^{(i)} \simeq N_i C_D P(\Delta E_i), \tag{3.17}$$

where N_i is the number of ith-nearest neighbor sites and P is the probability of that one ith-nearest neighbor site is occupied by a vacancy, which should be a function of pair binding energies and free vacancy concentration as:

$$P(\Delta E_i) = \frac{C_V^0 \exp(\Delta E_i/kT)}{C_S + C_V^0 \exp(\Delta E_i/kT)}. \tag{3.18}$$

Eq. (3.16) indicates that the $P(0) \simeq C_V^0/C_{Si}$ in the regions further than the $3nn$ site distance from any dopant atoms and $P(\Delta E_x \to \infty) \simeq 1.0$ for extremely heavily-doped areas, by which probability the site would always be occupied by vacancy.

For a vacancy associated with two dopant atoms at the nearest neighbor sites, we need to consider additional conditions including two-dopant configurations. The second order approximation is

$$C_V^{(i,j)} \simeq N_i N_j \left(\frac{C_D^2}{C_S}\right) P(\Delta E_i + \Delta E_j). \tag{3.19}$$

Considering the contributions from all possible approximation orders $C_V^{\text{total}} = C_V^{1st} + C_V^{2nd} + \ldots$, we have the total vacancy concentration expressed as

$$\frac{C_V}{C_S} \simeq \sum_i N_i \left(\frac{C_D}{C_S}\right) P(\Delta E_i) + \sum_{i \neq j} N_i N_j \left(\frac{C_D}{C_S}\right)^2 P(\Delta E_i + \Delta E_j) + \ldots. \tag{3.20}$$

This implies that the effect hop rate ν_{eff}, which is proportional to C_V/C_S, can also be expanded in the power series of $(C_D/C_S)^n$. Therefore, from Eq. (3.1) and Eq. (3.19), the diffusivity in the heavily-doped materials, can be expected to have a polynomial form:

$$\frac{D}{D_{\text{self}}} = \left(\frac{D^{\text{int}}}{D_{\text{self}}}\right) [1 + \beta_1 \left(\frac{C_D}{C_S}\right) + \beta_2 \left(\frac{C_D}{C_S}\right)^2 + \ldots] \tag{3.21}$$

where $D^{\text{int}}/D_{\text{self}}$ is the normalized diffusivity in moderately-doped material expressed by Eq. (3.13), which is only dependent on C_V^0 and binding energies. Coefficients β_i

rely on averages over interactions of vacancies with $i+1$ dopant atoms. The values of the β_i could potentially be calculated by summing over all the different lattice structure configurations with $i+1$ dopant atoms and all possible vacancy numbers with appropriate weight factors. However, we choose to attack the problem using Monte Carlo simmulations described in the following chapters.

Chapter 4

Monte Carlo Lattice Simulations

Since Flinn and McManus [30] reported the first comprehensive Monte Carlo simulations based entirely on a postulated solid-state diffusion process, many papers have followed on using Monte Carlo simulations to deal with diffusion-related topics. However, there is a carefully drawn distinction between the Monte Carlo calculations of defect formation energies in continuous space system [31], and the Monte Carlo random-walk calculations which are based implicitly on discrete hopping models. The only common feature of these two Monte Carlo calculations is the use of machine-generated random numbers. The application of the first Monte Carlo calculations is basically for the numerical evolutions of configurational integrals, the numerical solutions of interaction energy equations from quantum physics theories, and so on [31, 33]. In this research, I use the latter calculations, i.e. the Monte Carlo random-walk calculations, to trace both the dopant atoms and vacancies during the diffusion through the three-dimensional silicon lattice structure.

4.1 Basic Considerations

There are several basic issues to consider in developing a C-language program for Monte Carlo lattice simulation.

4.1.1 Simulation Lattice

As we know, silicon crystallizes in the diamond lattice structure. The cubic unit cell of three-dimensional diamond lattice is pictured schematically in Figure 4.1. Within one cubic cell of Figure 4.1, there are eight atoms marked by solid circles while the atoms of adjacent cells are marked by dashed circles. Therefore, the three-dimensional diamond lattice can be constructed from 8-site basis unit cells in the simulation program.

As depicted in Figure 4.1, the eight atom sites within the unit cell are labeled

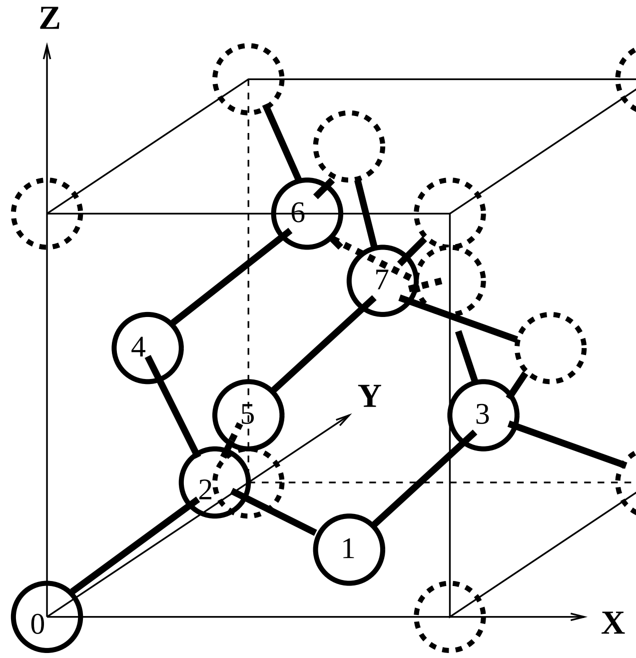

Figure 4.1: The cubic unit cell of diamon lattice structure with a three-dimensional view, where the tetrahedral lines represent for selective bonds between atoms.

from "0" to "7". In order to locate the atoms and vacancies more efficiently, a four-dimensional array $\{N_x, N_y, N_z, n\}$ is used for the position of lattice sites, i.e. N_i for i-axis position of the unit cell corresponding to site "0" and n for the nth site inside the unit cell. Within the unit cell, the displacement from site "0" to site "n" has its own projections Δx_n,Δy_n and Δz_n along X, Y and Z axis. Thus, $\{N_x, N_y, N_z, n\}$ gives the coordinates of each lattice site $\{N_x + \Delta x_n, N_y + \Delta y_n, N_z + \Delta z_n\}$.

In order to get a good statistical result, the lattice size of the $N_x \times N_y \times N_z$ array of cubic cells is chosen to guarantee numbers of both dopant atom and vacancy sites larger than 200 for each simulation group. The total number of unit cell used for simulations varied strongly with the dopant density from 10^4 to 10^7.

Because of the limitation of the computer facility used, a large simulation lattice size could still be insufficient to represent the size of the real diffusion system. Thus, periodic boundary conditions are used for the simulation lattice. Once a dopant atom or a vacancy crosses the edge of the $N_x \times N_y \times N_z$ lattice, it can continue hopping starting from the opposite edge along the same direction with the same nearest neighbors. Such a computational operation is called *lattice-continuation* in this paper. The *lattice-continuation* must be recorded by the program to calculate the total distance of hopping.

4.1.2 Binding Energy Terms

In this research, we assume that the binding energies exist only between the dopant atoms and vacancies. Interactions among vacancies and among dopant atoms are neglected.

Now, we consider how the binding energies affect the simulations. As discussed in the atomistic model of Chapter 3, I consider only the binding energies within a range of the $3nn$ site distance. Eq. (3.8) shows that value of binding energy is decreased as the distance is increased between the dopant atom and the vacancy. The binding energies between the dopant atom and the 1st-, the 2nd- and the 3rd-nearest neighboring vacancies are $\Delta E_1, \Delta E_2$ and ΔE_3. These energies are positive to represent an attraction between the vacancy and the dopant atoms. At lattice site i, one vacancy has the binding energies contributed from any dopant atoms at all possible neighboring sites as

$$\Delta E_i \quad = \quad n_{1nn}\Delta E_1 + n_{2nn}\Delta E_2 + n_{3nn}\Delta E_3, \tag{4.1}$$

where n_{1nn} is the number of dopants at the 1st-nearest neighbor sites, n_{2nn} for the 2nd-nearest neighbor and n_{3nn} for the 3rd-nearest neighbor.

In order to calculate the system energy, the program requires a memory of the silicon lattice structure, i.e. for any site, the program is able to get the coordinates of all four 1st-nn sites, twelve 2nd-nn sites and twelve 3rd-nn sites. The binding energies are calculated after the program searches and distinguishes the species at neighboring sites radiated from a central site i.

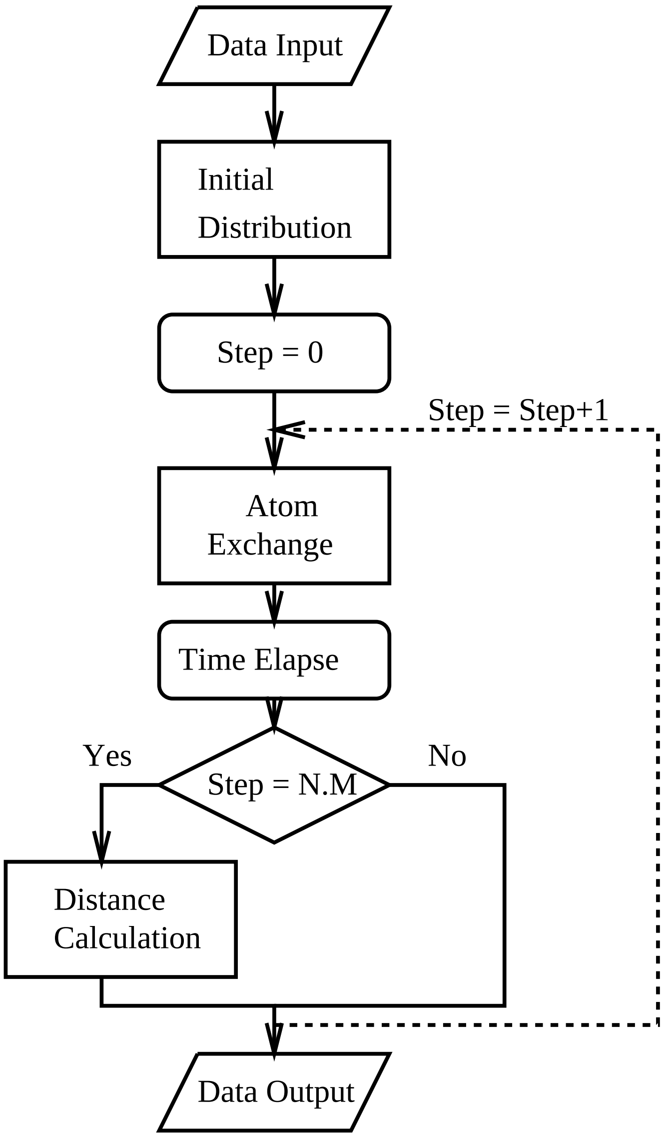

Figure 4.2: The block diagram of main program of the Monte Carlo simulations.

4.2 Implementation of the Simulations

The program discussed in this section is for uniformly distributed vacancies and dopant atoms. For the simulations of dopant diffusion caused by a vacancy gradient, the program requires some modification to allow a non-uniform distribution of vacancies, which will be introduced in Chapter 6.

The Monte-Carlo simulations are implemented by a C-language program. Figure 4.2 shows a block diagram of main program.

4.2.1 Structure Declaration

According to the mechanism of dopant-vacancy pair diffusion, the motion of a dopant atom relies upon exchanging sites with an adjacent vacancy. For each simulation step, a vacancy exchanges its lattice site with either dopant, silicon or another vacancy. In order to trace the positions of dopant atoms and vacancies after every vacancy hopping step, the program needs effective data structures.

In the program, two important data structures are required simultaneously to record the site location of each labeled dopant atom and vacancy and to store the species (i.e., dopant, silicon or vacancy) of each lattice site. These two structure declarations are as follows:

```
typedef struct atom{
int x, y, z, n, ix, iy, iz;
float energy;
} ATOM;
...
typedef struct connect{
int neigh[8]; } CONNECT;
...
CONNECT ***matrix-LATTICE(A,B,C)
int A, B, C;
{
```

```
int i, j;
CONNECT ***m;
m = (CONNECT***) malloc((unsigned)C*sizeof(CONNECT**));
for (i=0; i<C; i++)
m[i] = (CONNECT**) malloc((unsigned)A*sizeof(CONNECT*));
for (i=0; i<C; i++) {
for (j=0; j<A; j++) {
m[i][j] = (CONNECT*) malloc((unsigned)B*sizeof(CONNECT));
} }
return m;
}
```

The first type structure is for dopant atom array and vacancy array. Once the total numbers of dopant atoms and vacancies are known, the structure ATOM is able to label each dopant or vacancy with its members, i.e. site coordinates $\{N_x, N_y, N_z, n\}$ and the numbers of lattice-continuation along three axes $\{ix, iy, iz\}$. The second type structure CONNECT defines a four-dimensional pointer matrix, $LATTICE[x][y][z].n$ used for $A \times B \times C \times 8$ lattice sites. Based on whether a dopant atom, a silicon atom or a vacancy is at the ith site $\{x_i, y_i, z_i, n_i\}$, the corresponding pointer in the matrix $LATTICE[x_i][y_i][z_i].n_i$ is assigned to the address of character "D", "S" or "V" respectively.

When the program is calculating the total binding energies associated with a vacancy, $LATTICE[x][y][z].n$ is used for the vacancy to search for how many dopant atoms are located within the third-nearest neighbor distance.

Both $LATTICE[x][y][z].n$ and ATOM are used to calculate all possible vacancy hopping rates. For any vacancy, the hopping rate is decided by the change of system energy as in Eq. (3.8). Once the vacancy location is checked by ATOM, a subroutine finds the locations of all $1nn$, $2nn$ and $3nn$ sites. These neighboring sites are checked by $LATTICE[x][y][z].n$ to search for the dopant atoms and therefore, the total dopant/vacancy pair binding energies can be calculated from the number of neighboring dopants with different site distances. The same operation is applied to situations in which the vacancy is assumed to have site-exchange with one of the adjacent atoms. Thus, the program is able to get all possible changes of system energies associated with all possible vacancy site-exchanges by running through all the elements in the ATOM vacancy array.

When site-exchange is operated, the lattice site species $LATTICE[x][y][z].n$ and ATOM array for both dopants and vacancies are updated to complete one step of the simulation.

4.2.2 Initial Set-up

Before the Monte Carlo random walk begins, it is necessary to assign the occupation of all lattice sites (i.e., silicon atoms, dopants and vacancies), based on the equilibrium concentrations. The initial distribution of the dopant atoms can be specified from the *Data Input.* The input data include (1) the distribution type of dopant atom, i.e. a normal distribution along the principle direction (z-axis) of the diffusion with uniform distribution in X and Y dimensions or uniform distributions in all three dimensions; (2) the lattice size $A \times B \times C$; (3) the concentration of free vacancies and the doping density and (4) the total number of random walk steps.

In the bulk of the simulations, a three dimensional uniform distribution of dopant atoms was used. While a dopant atom is at the lattice site, it will always attract vacancies to its neighboring sites. Depending on the dopant density and the binding energies, the total vacancy concentration C_V will be higher than C_V^0. After the dopant atoms are distributed throughout the silicon lattice, the vacancy can be seeded according to the probability given by

$$P(\Delta E_i) \quad = \quad \frac{C_V^0 \exp[\Delta E_i/kT]}{C_S + C_V^0 \exp[\Delta E_i/kT]} \tag{4.2}$$

where the total binding energy ΔE_i is from Eq. (4.1) and C_V^0 is the vacancy concentration at the sites farther than the third-nearest neighbor distance from any dopant atoms. Every silicon atom site is checked with $P(\Delta E_i)$ and if $P(\Delta E_i)$ is equal to or larger than the machine-generated random number between 0 and 1, the site will be replaced by a vacancy.

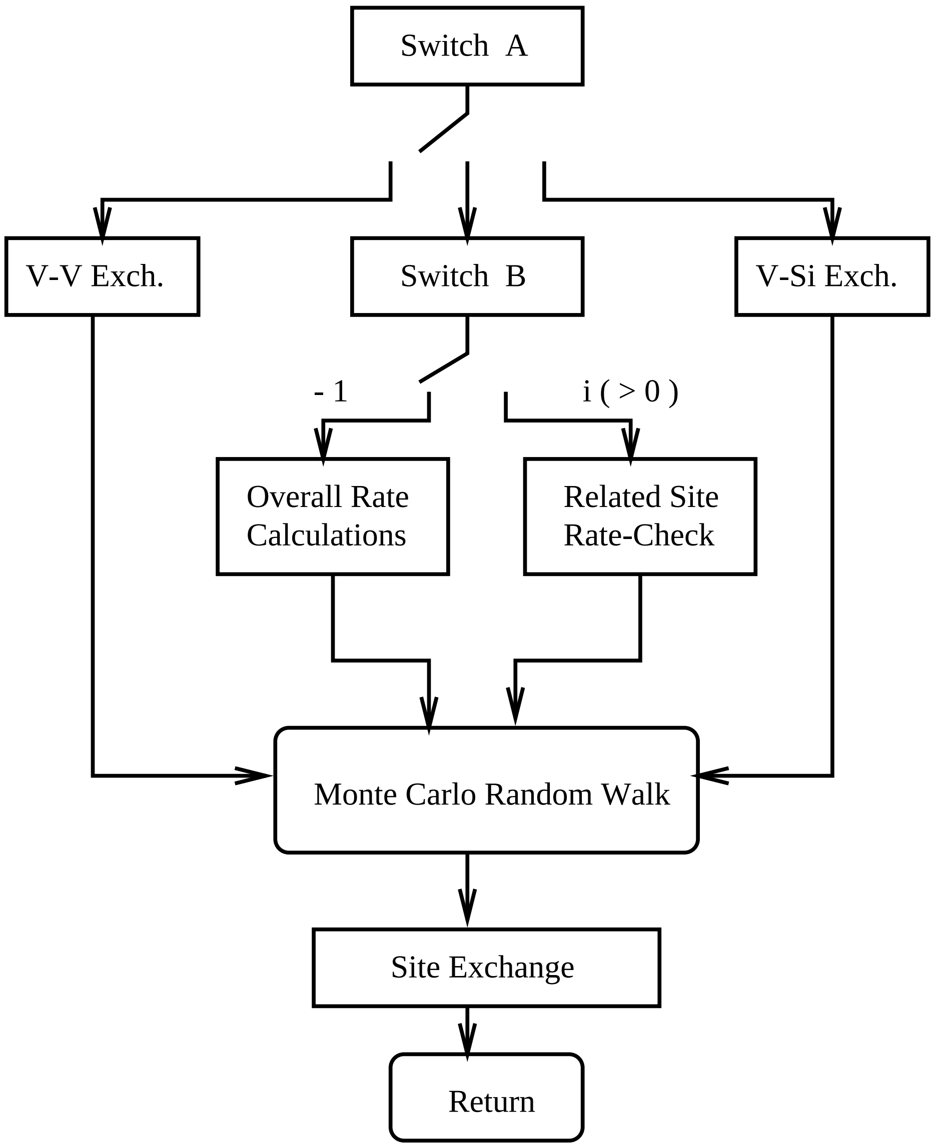

Figure 4.3: The block diagram of major subroutine of Monte Carlo simulations.

4.2.3 Monte-Carlo Random Walk Subroutine

Every step of the Monte Carlo random walk is executed by the subroutine *Atom-Exchange* whose block diagram is shown in Figure 4.3. At each step, a vacancy exchanges sites with a dopant atom, a silicon atom or another vacancy. The hopping of a vacancy (in simulation, the vacancy behaves as a particle) is determined by a machine-generated random number. Thus the hopping of vacancies is the central kinetic process of the Monte Carlo simulations.

The vacancy hopping rates are biased by changes of system energy associated with a prospective hop. The rate is given by:

$$\nu \;=\; \nu_V^0 \exp\left(-\frac{\Delta E_{\text{final}} - \Delta E_{\text{initial}}}{2kT}\right), \tag{4.3}$$

where ΔE_{final} and $\Delta E_{\text{initial}}$ are the final and initial system energy respectively, which are calculated from minus the summation of all vacancy-associated binding energies (positively-valued) in Eq. (4.1). The change of system energy comes from the changing neighborhood of the vacancies. Consequently, if a vacancy exchanges with a dopant atom, after the hop the displacement of that dopant atom will further change the system energy if there are other vacancies within an interaction distance.

For each simulation step, one vacancy exchanges the site with one of its four adjacent atoms or vacancies. If the total vacancy number is N_V, each single simulation step has $4 \times N_V$ possible site exchanges. The simulation program needs to have $4 \times N_V$ hop rates ν_k calculated from Eq. (4.3), and then uses a machine-generated random number to decide which particular site-exchange k occurred during this step.

At the very beginning of random walk simulations, Switch A and Switch B in the subroutine set the initial calculation of all $4 \times N_V$ possible hopping rates of Eq. (4.3). However, after the random walk begins, it is not necessary to recalculate all $4 \times N_V$ hopping rates step by step, but just to update those rates which are affected by the last site-exchange.

According to the last site-exchange, Switch A selects one of three options: (1) after a vacancy/dopant site-exchange, via Switch B, the hopping rates of all vacancies within interaction distance are recalculated; (2) after a vacancy/silicon site-exchange, only the four hopping rates of this vacancy need updates and (3) after a vacancy/vacancy site-exchange, none of $4 \times N_V$ hopping rates needs change, but the labels of these two vacancies should be exchanged.

The core part of the subroutine *Monte Carlo Random Walk* decides which one of the $4 \times N_V$ possible site-exchanges happens during this step. The rate of the ith vacancy hopping to its jth adjacent site is marked as $\nu_{m(i,j)}$ with label $m(i,j) = 4i+j$

($i = \{0, 1, ..., N_V - 1\}$ and $j = \{0, 1, 2, 3\}$). Once it gets a machine-generated random number η, the program determines that the kth site-exchange happen during this step by:

$$\frac{\sum_{m=0}^{k} \nu_{m(i,j)}}{\sum_{m=0}^{4N-1} \nu_{m(i,j)}} \leq \eta < \frac{\sum_{m=0}^{k+1} \nu_{m(i,j)}}{\sum_{m=0}^{4N-1} \nu_{m(i,j)}}. \tag{4.4}$$

where $0 \leq k \leq 4 \times N_V - 1$.

After $k = 4i + j$ is known, the procedure *Site-Exchange* specifies the ith vacancy exchanging with its jth adjacent sites and the species (dopant atom, silicon atom or another vacancy) involved in this site-exchange. The corresponding addresses in the vacancy array (and dopant array, if it is a vacancy/dopant site-exchange) are updated with new data after this site-exchange.

4.2.4 Data Output

Two more things are required to complete for every simulation step, time increment and data output. Assuming the simulations are Poisson processes, the elapsed time is related to the summation of hopping frequencies. The expected time for a single step is given by

$$\Delta t = [\sum_{m=0}^{4N-1} \nu_{m(i,j)}]^{-1}. \tag{4.5}$$

The total elapsed time is accumulated from Δt of each step.

The dopant diffusivity is the final quantity we want to measure from the simulations. From the theory of random walks [36], the diffusivity is given by:

$$D = \langle | \Delta\vec{d} |^2 \rangle / 6t, \tag{4.6}$$

where $\Delta\vec{d}$ is the displacement for a dopant atom during the time interval t. The initial coordinates of all dopant sites are stored in ATOM-type structures. To check the diffusivity, the displacement and other related quantities must be calculated via a comparison of the current dopant positions to the initial ones. To save CPU time, it is not necessary to calculate the displacement every step. The condition $Step = N \times M$ is set in main program so that the essential data are recorded in an output file periodically after certain amount of steps, which is typically 50,000 or 100,000 steps in the simulations. This finishes the cycle of one simulation step.

The next step of vacancy hopping will begin after the vacancy and dopant distribution are updated and the hopping rates are recalculated within the neighborhood of the last hop. The loop continues until the desired total number of steps have been completed.

Chapter 5

Results and Discussions

In this section, we begin by specifying the values of binding energies used in the simulations. Next we discuss initial tests of the Monte Carlo simulation program. Finally, comparing to the predictions from atomistic model and other related analyses and experimental observations, we discuss the simulation results for both moderate doping diffusion and heavy doping diffusion.

5.1 The Pair Binding Energies and Free Vacancy Concentration

To choose appropriate values of pair binding energies $\{\Delta E_1, \Delta E_2, \Delta E_3\}$ is important for the simulations. As shown in Figure 3.1 and Eq. (3.8), the values of binding energies decrease as the distance between dopant and vacancy increases. As a rough estimate, the values of binding energies used in this research are assumed to have following relationship:

$$\frac{\Delta E_2}{\Delta E_1} = \frac{2}{3}; \qquad \frac{\Delta E_3}{\Delta E_1} = \frac{1}{3}. \tag{5.1}$$

In the simulations, the first nearest neighboring dopant-vacancy binding energies use experimental values of the binding energy of vacancies with arsenic (1.23eV) and with phosphorus (1.04eV) [35]. The interaction energies with different pairing distances are then given by the relationships of Eq. (5.1).

The concentration of free vacancy C_V^0 is chosen for the simulations in order to balance two concerns. Based on metal diffusion data [37], the intrinsic vacancy concentration at 1050^oC is around $3 \times 10^{15}\mathrm{cm}^{-3}$. Such low concentrations represent a dilute solution and the dopant/vacancy pair density and thus the dopant diffusivity can be expected to be a linear function of free vacancy concentration. Since our results are normalized, any small densities of free vacancies should give the same results. On the other hand, smaller values of C_V^0 require a larger lattice size $N_x \times N_y \times N_z$ for simulations to have enough vacancies for reliable results and therefore, a longer CPU time to run the program. Saving CPU time leads to use of a high concentration of free vacancies. Thus, we must pick a value of free vacancy concentration to optimize the CPU time savings without sabotaging the conditions for dilute solution approximation.

Based on the limits of linearity of the doping density with C_V^0, $C_V^0 = 5.0 \times 10^{16}\mathrm{cm}^{-3}$ was chosen for the diffusion simulations, including simulations of dopant flux caused by a vacancy gradient in Chapter 6.

5.2 Testing of the Monte Carlo Simulations

An important test for the Monte Carlo simulations is to verify that the machine-generated random numbers lead to a desired distribution of dopant atoms or vacancies. The simple way to do this is to generate a lot of random numbers, and then count these numbers in the divided areas. The frequency of random numbers appearing in a particular area is equal to the geometry size ratio of this area to the whole area. An alternative way to check the distribution of random numbers in these simulations is to count the number of vacancies in different dopant-vacancy pairing configurations, and make a comparison to the predicted results from the analytic calculation.

As analyzed in Chapter 3, a dopant atom has higher vacancy concentration in its neighborhood than in the remote area. The first order approximation of the concentration of vacancy within a particular distance from a dopant is given by

$$C_V^{(i)} = N_i C_D [\frac{C_V^0 \exp(E_i/kT)}{C_S + C_V^0 \exp(E_i/kT)}], \tag{5.2}$$

where i represents the ith nearest neighbor site of the dopant atom, N_i is the number of the ith nearest neighbor sites and E_i is the binding energy. The three compositions of i are $\{100\}$ for one vacancy at the $1nn$ site, $\{010\}$ for one vacancy at the $2nn$ site and $\{001\}$ for one vacancy at the $3nn$ site. The second order approximation of vacancy concentration represents for vacancies associated with two dopants at $i$nn site and $j$nn site respectively, which is

$$C_V^{(i,j)} = N_i N_j \left(\frac{C_D^2}{C_S}\right) \{\frac{C_V^0 \exp[(E_i + E_j)/kT]}{C_S + C_V^0 \exp[(E_i + E_j)/kT]}\}. \tag{5.3}$$

For the second order approximation, I just picked as an example $(i,j) = \{101\}$ which represents the vacancy associated with one dopant at 1st-nn site and another dopant at the 3rd-nn site.

C_D		$C_V^{\{100\}}$	$C_V^{\{010\}}$	$C_V^{\{001\}}$	$C_V^{\{101\}}$
0.001	mod.	5.6×10^{-4}	3.57×10^{-5}	6.5×10^{-7}	2.26×10^{-5}
	simu.	5.3×10^{-4}	4.1×10^{-5}	5.67×10^{-7}	2.0×10^{-5}
0.0001	mod.	5.6×10^{-5}	3.57×10^{-6}	6.5×10^{-8}	2.26×10^{-7}
	simu.	5.3×10^{-5}	4.05×10^{-6}	4.05×10^{-8}	2.9×10^{-7}
0.00001	mod.	5.6×10^{-6}	3.57×10^{-7}	6.5×10^{-9}	2.26×10^{-9}
	simu.	5.0×10^{-6}	3.7×10^{-7}	6.3×10^{-9}	≈ 0

Table 5.1: The concentrations of paired vacancies from Eq.(5.1) and Eq.(5.2) and from the Monte Carlo simulations with C_D and C_V in the units of C_{Si}.

In the simulations, we set the program to count the number of vacancies in different configurations. The calculation results from Eq.(5.1) and Eq.(5.2) are compared to the simulation results in Table 5.1, which verifies the reliability of the simulation program.

5.3 Diffusivity for Moderately-Doped Materials

In Chapter 4, it was mentioned that the dopant diffusivity can be calculated from the simulation output of average square displacement after a certain number of hopping steps., i.e.

$$D = \langle \mid \Delta\vec{d} \mid^2 \rangle / 6t, \tag{5.4}$$

where t is the time interval. Tracing the coordinates of all dopant atoms from step to step, we expect that for a fixed doping density, vacancy concentration and binding energies, $\langle \mid \Delta\vec{d} \mid^2 \rangle$ should be a linear function of the time. The slope of this function can be calculated from the simulation results by linear regression. Dividing the slope by 6, we can get the dopant diffusivity.

Figure 5.1 shows that for fixed doping density $C_D = 5.0 \times 10^{18}\text{cm}^{-3}$, Monte Carlo simulations were applied to the systems corresponding to three sets of pair binding energies. Despite a small amount of noise, the average displacement square $\langle \mid \Delta\vec{d} \mid^2 \rangle$ shows good linearity in the time domain. With Eq. (5.3), the dopant diffusivity can be easily calculated from the simulations.

Now, we check the simulation results with the coefficient of self diffusion in Eq. (3.4). If we set the pair binding energies as $\{0, 0, 0\}$ in the simulations, the dopant atoms become tracers for self-diffusion. Normalized by lattice constant and the hopping rate of free vacancy, the self-diffusion coefficient is $D^0_{\text{self}} = C^0_V/(16C_S)$. With $C^0_V/C_S = 1.0 \times 10^{-4}$, we have simulation results of $6.4 \times 10^{-6}(\nu^{0\ -1}_V a^{-2})$ compared to the calculation result of $6.25 \times 10^{-6}(\nu^{0\ -1}_V a^{-2})$.

Based on the binding energies and the free vacancy concentration $C^0_V = 5.0 \times 10^{16}\text{cm}^{-3}$, the simulations were applied to lightly/moderately doped materials. From the analyses in Chapter 3, for doping density $C_D < 2.0 \times 10^{20}\text{cm}^{-3}$, the dopant diffusivity normalized by the self-diffusion coefficient of Eq.(3.4) is given by

$$\frac{D}{D_{\text{self}}} = \frac{8C_S \langle \mid \Delta\vec{d} \mid^2 \rangle}{3C^0_V t}. \tag{5.5}$$

On the other hand, the atomistic model expressed the dopant diffusivity normalized

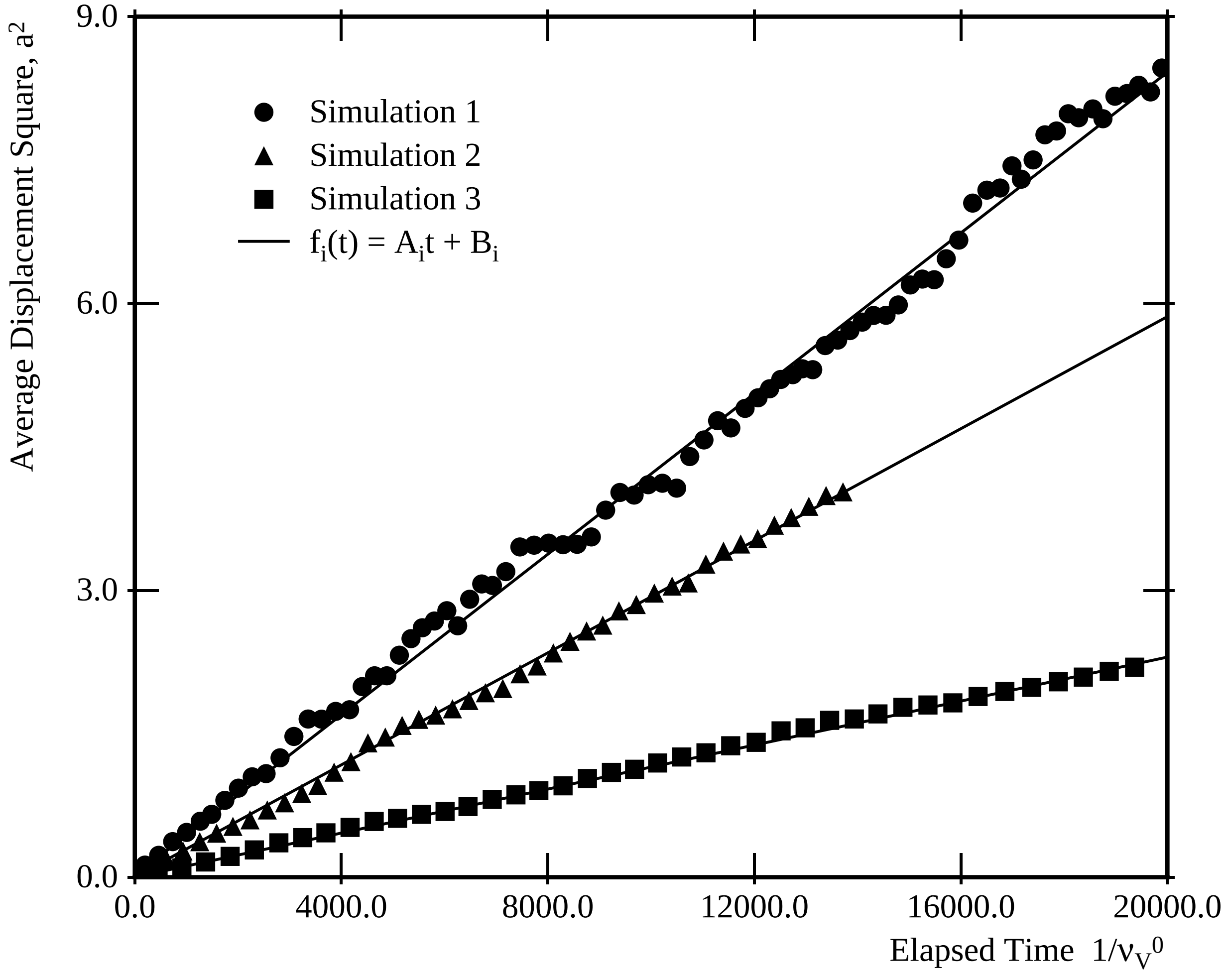

Figure 5.1: The average square displacement versus elapsed time for three simulation data groups with different binding energies and $C_D = 5.0 \times 10^{18}$cm^{-3}, where $f_i(t)$ is the fitting curve with slope A_i for the ith simulation and elapsed time is in the unit of $1/\nu_V^0$.

by the self-diffusion coefficient as

$$\frac{D}{D_{\text{self}}} = 3\exp(\frac{\Delta E_{2nn}+\Delta E_{3nn}}{2kT}). \tag{5.6}$$

To make a comparison between the atomistic model and the Monte Carlo simulation results, the diffusivities using both Eq. (5.5) and Eq. (5.6) are listed in Table 5.2.

Binding Energies (unit: $2k$T)	Analytic Cal.	C_D in unit of cm^{-3}			
		5×10^{17}	5×10^{18}	1.5×10^{19}	5×10^{19}
	Dopant Diffusivity Normalized by D_{self} of Eq. (3.4)				
$E_1\{6,4,2\}$	1.21×10^3	1.16×10^3	1.11×10^3	1.18×10^3	1.19×10^3
$E_2\{5.4,3.6,1.8\}$	6.64×10^2	7.62×10^2	7.79×10^2	7.84×10^2	6.81×10^2
$E_3\{4.56,3.04,1.52\}$	2.87×10^2	$3.2\times10^2*$	3.07×10^2	2.75×10^2	2.51×10^2

Table 5.2: For the moderate-doping densities, the dopant diffusivities from the Monte Carlo simulations Eq. (5.6) and the analytic calculations using Eq. (5.7) for three binding energy groups with a fixed free vacancy concentration $C_V^0 = 5\times10^{16}$cm^{-3}. The simulation* used $C_D = 1.0\times10^{18}$cm^{-3}.

The simulation results in Table 5.2 show a good match to the analytic calculations from Eq. (3.14) and demonstrates a consistency with the fact that for moderately doped materials, dopant diffusivity normalized by the self-diffusion coefficient is independent of the doping density and can be accurately predicted by the atomistic model proposed in Chapter 3. In addition, the reliability of the simulation program has been confirmed once again by the data of Table 5.2.

5.4 Heavy Doping Effects

Keeping other conditions fixed but increasing the doping density, the simulations were also run for the heavily-doped systems. From Eq. (5.5), the diffusivity is determined from the simulations. In Figure 5.2, the doping density spans a wide range

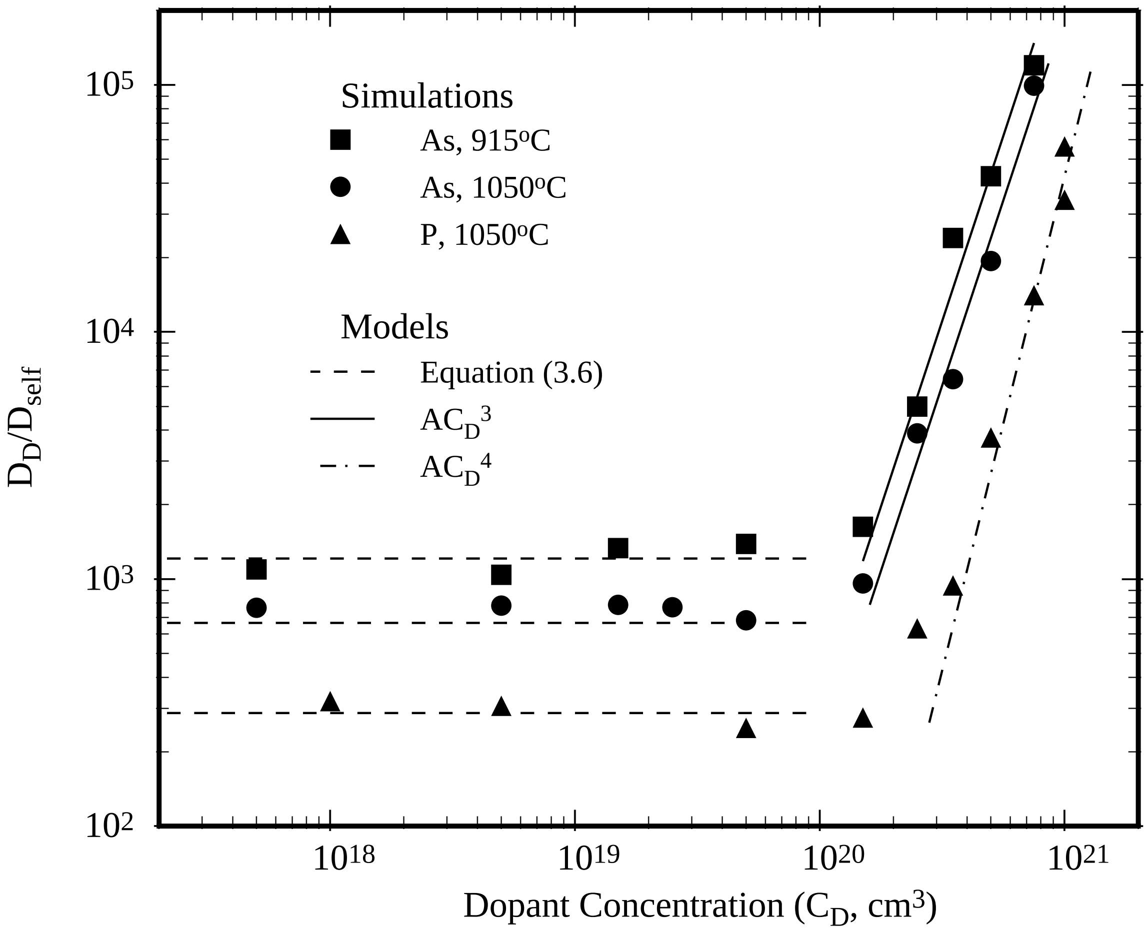

Figure 5.2: The normalized diffusivity versus doping density where the dopant-vacancy pair binding energies are based on the binding energy of arsenic at 915^oC and 1050^oC and of phosphorus at 1050^oC.

from $1.0 \times 10^{18}\text{cm}^{-3}$ to $1.0 \times 10^{21}\text{cm}^{-3}$. Figure 5.2 shows clearly that for each set of binding energies, the dopant diffusivity normalized by the self-diffusion coefficient always undertakes a transition from independent of doping density to strongly dependent on doping density when the doping density becomes larger than a threshold value.

As we see in Fig 5.2, when the doping density is above $2.0 \times 10^{20}\text{cm}^{-3}$, the diffusivity increases dramatically with increasing doping doping densities. Similar results were experimentally observed by Nylandsted Larsen *et al* [10, 28, 29] in silicon heavily doped with phosphorous.

As discussed in Chapter 2, in n-type silicon, donors diffuses predominantly via singly-charged vacancies [18, 27]. Thus, the effective diffusivity based on the Fermi-level effects is given by

$$D_{\text{eff}} \simeq D^{-}(\frac{n}{n_i}), \tag{5.7}$$

where D^{-} is the dopant diffusivity due to negatively-charged vacancies and n is electron concentration which is approximately equal to the doping density C_D. The dependence on doping density in Eq. (5.7) arises from changes in the free vacancy concentration due to the Fermi level shift.

However, for the heavy-doping diffusion as our simulation results show in Figure 5.2, the diffusion model based on Fermi level effect is no longer sufficient to predict the trend of rapid increase in the normalized dopant diffusivity. The diffusivity expression should be modified model to:

$$D = D^{-}(\frac{n}{n_i})(1+\kappa). \tag{5.8}$$

As analyzed in Chapter 3, κ in Eq. (5.8) is contributed from the enhancement of dopant diffusion due to the reduction of vacancy migration barrier in the heavily-doped materials. From the simulation results of heavy-doping diffusion in Figure 5.2, the dopant diffusivity normalized by the self-diffusion coefficient D_{self} becomes proportional to the third to fourth power function of the doping density when the doping density is higher than the threshold C^{*}. The simualtion results of a rapid increase in normalized diffusivity indicates that $\kappa \simeq (C_D/C^{*})^{n}$. Therefore, the effective diffusivity can be expressed as

$$D = D^{-}(\frac{C_D}{n_i})[1 + (\frac{C_D}{C^*})^n], \qquad (5.9)$$

where n_i is the intrinsic carrier density and C^* is the threshold value of doping density to trigger the heavy-doping effects.

In order to compare to the experimental observations, the linear term in Eq. (5.9) is fitted with the experimental data from both Fair [18] and Nylandsted Larsen [10] for $C_D < 10^{20}\text{cm}^{-3}$. Taking the data for phosphorus at 1050°C, we have C^* as $2.9 \times 10^{20}\text{cm}^{-3}$ and n as 4 (3.5 for arsenic form the experiment [10]). Then we exptrapolate the curve from Eq. (5.9) in Figure 5.3, which shows that our model can predict the diffusivity in heavily doped materials in a good agreement with the experimental results.

One important note is that the data used by Nylandsted Larsen *et al.* [10] are for arsenic tracer diffusion in phosphorus-doped systems and thus, phosphorus is a more decisive doping material. Therefore, in the diffusivity expression of Eq. (5.9), we use C_D, C^* and n corresponding to the data from phosphorus-doping diffusion. As shown in Figure 5.2, C^* seems to depend weakly on the binding energies. As discussed in Chapter 3, the major impact on the transition to heavy-doping effect is from the doping density. Once a vacancy is associated with more than one dopant at the same time, the potential barrier for vacancy migration will be lowered. When the pair binding energies increase as for arsenic relative to phosphorus, the energy barrier is reduced and C^* will slightly decrease.

5.5 A Short Comment on Percolation Model

In order to explain the heavy-doping diffusion, Mathiot and Pfister proposed a percolation model [7]. In this model the effective diffusivity is represented by two terms, the normal diffusivity $D^{\{\mathrm{n}\}}$ and the percolation diffusivity $D^{\{\mathrm{p}\}}$. The normal doping diffusion, $D^{\{\mathrm{n}\}}$ is based on diffusion via neutral and single negatively charged vacancies expressed in the previous chapters.

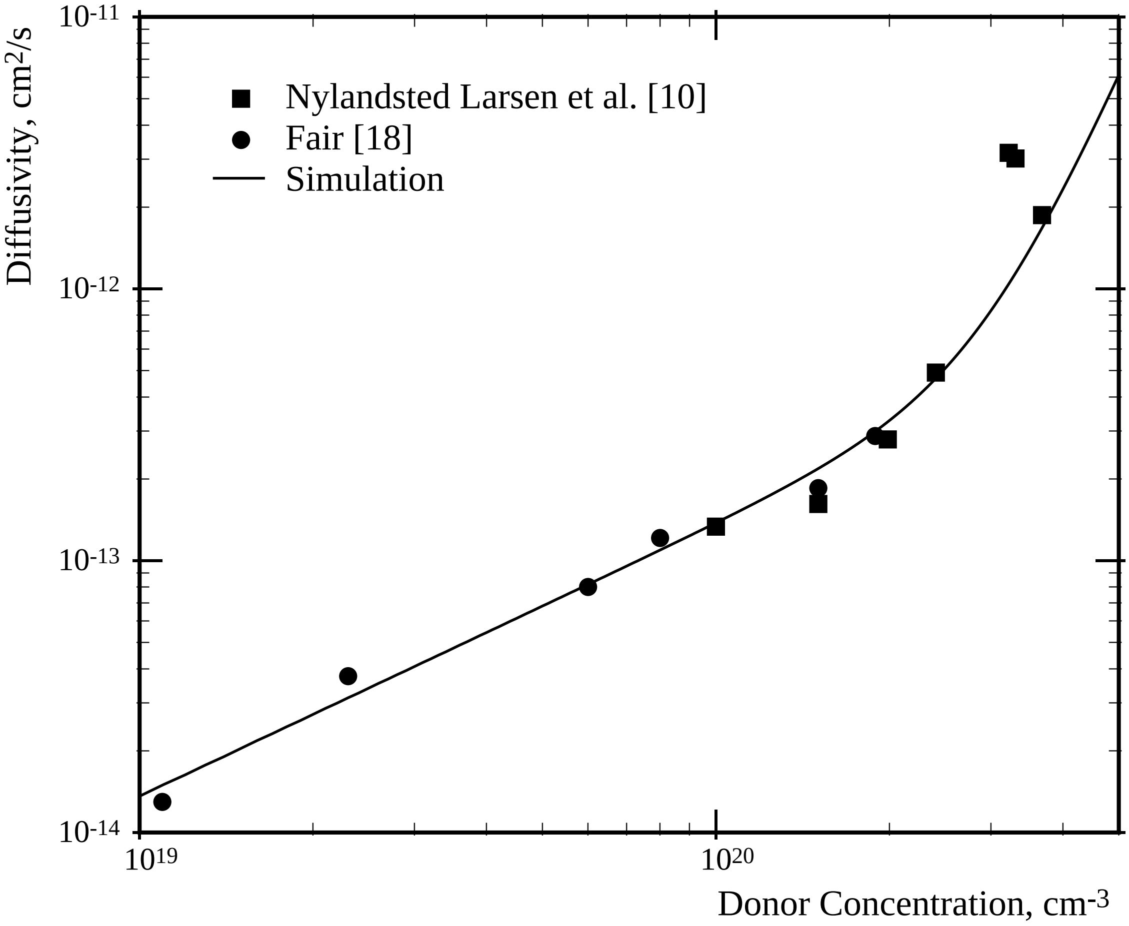

Figure 5.3: Comparison of experimental measurement of arsenic diffusivity at 1050^{o}C versus doping densities to the curve predicted from the results of Monte Carlo simulations.

As doping density increases, the dopant-vacancy pair diffusion is replaced by the percolation of dopant-vacancy cluster. The $D^{\{\mathrm{p}\}}$ is determined by the Fermi level effect as:

$$D^{\{\mathrm{p}\}} \;=\; FD^{-}\frac{n}{n_i} = FD^{\{\mathrm{n}\}} \qquad (5.10)$$

where $F = \exp(E_B/kT)$ and E_B is the reduction in migration energy barrier for vacancy as the doping density increases in multiple dopant-vacancy cluster. In this research, $E_B = \Delta E_3$ as shown in Figure 3.3. The percolation model has the effective

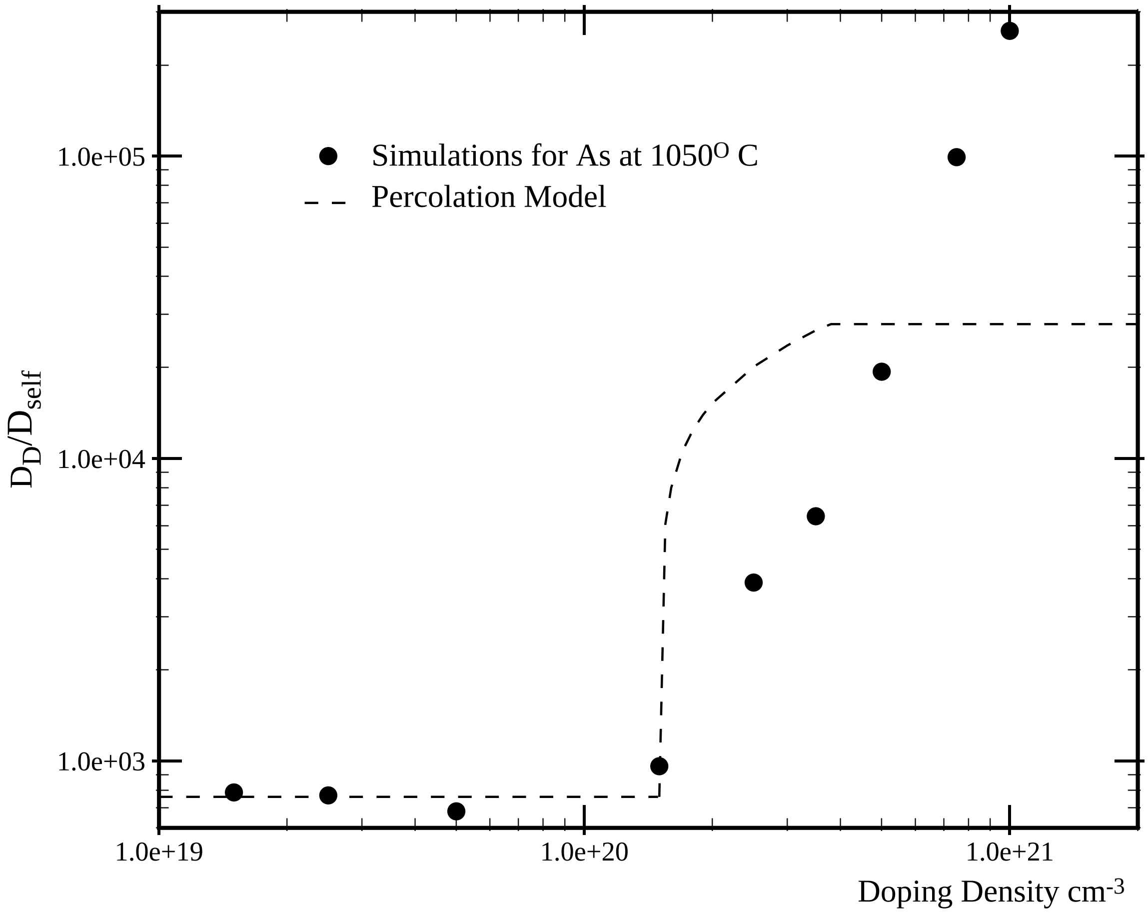

Figure 5.4: Comparison of simulation results of arsenic diffusivity at 1050^oC versus predicted curves from the percolation model.

dopant diffusivity as

$$D_{\text{eff}} = (1 - P_\infty) D^{\{\text{n}\}} + P_\infty D^{\{\text{p}\}}, \tag{5.11}$$

where P_∞ is the probability that an impurity belongs to the percolation cluster with

$$\begin{aligned} P_\infty(C_D \leq C^*) &= 0; \\ P_\infty(C_D > C^*) &= \min\{1, K[(\frac{C_D}{C^*}) - 1]^\beta\}. \end{aligned} \tag{5.12}$$

where $\beta = 0.4$ and $K = 0.85$ [8].

As an application of percolation model to this research, $D^{\{\text{n}\}}$ is equal to the diffusivity of moderate-doping diffusion in Eq. (3.13) and the effective diffusivity expression from the percolation model is

$$\frac{D}{D_{\mathrm{self}}} = 3\exp\left(\frac{\Delta E_2 + \Delta E_3}{2}\right)[(1-P_\infty) + P_\infty \exp\left(\frac{\Delta E_3}{kT}\right)], \tag{5.13}$$

where D_{self} is from Eq. (3.4).

A curve based on percolation model is plotted in Figure 5.4 with a comparison of simulation results for arsenic at 1050^oC. The percolation curve has a characteristic jump and the derivative $\partial D_{\mathrm{eff}}/\partial C_D$ is not a continuous function of C_D at the threshold in Figure 5.4. The physical explanation of this percolation phenomenon is that as doping density increases above the threshold, the dopant-vacancy pairs are suddenly replaced by an irregular network of dopant-vacancy strings in the silicon lattice. The dopant diffusivity based on this network is not a continuous function of doping density, but rather dominated by the percolation probability of Eq. (5.14).

Our simulation results show that percolation model is not valid. As explained by atomistic model in Chapter 3, the enhancement of dopant diffusivity in heavily-doped material is dependent on the lowering of the energy barriers of vacancy migration. The barrier is gradually reduced by the continuously increasing doping density. Thus, once a vacancy has interactions with multiple dopant atoms, the dopant diffusivity should remain a continuous function of doping density.

Chapter 6

Vacancy Gradient and Dopant Flux

In the previous sections, we assumed a uniform distribution of vacancies. However, in many practical applications, it is important to understand how a gradient in the vacancy distribution affects the dopant diffusion process.

An interesting question about the dopant diffusion caused by a vacancy gradient is whether the dopant flux and vacancy flux will be in the same or opposite direction. As an example, if the dopant atoms are homogeneously distributed and the vacancy concentration increases with the depth from the surface, two possible fluxes of dopants are proposed. From the view of the pair diffusion mechanism [13], mobile pairs will form proportional to the vacancy concentration and diffuse in their gradient towards the surface. Thus, the flux of dopants is predicted in the same directions as the flux of the vacancies. However, Maser [14] suggested that dopant flux is opposite to the flux of vacancies based on the fact that dopant and vacancy have opposite direction of the displacement during each the site-exchange. Recent research by List *et al.* [15] derived both pair model and atomistic model from the vacancy hopping mechanism with an attractive potential between the dopant and vacancy and found that two fluxes could either have the same or the opposite directions depending on the range and magnitude of the potential between the dopant atom and vacancy.

6.1 Simulation Methods

After some modification of the program used for the simulations described and discussed in the previous chapters, several Monte Carlo simulations to investigate the dopant flux caused by the vacancy gradient were run. The major concern for the modified program is how to set up conditions for the edges of $N_x \times N_y \times N_z$ lattice so that along the principle direction of the diffusion, the vacancy concentration will form a gradient.

To set-up and maintain the vacancy gradient, the program was modified by two steps. First, along the principle direction of the diffusion (called z-axis in the following), I applied a difference of vacancy concentration on the two surfaces of the lattice block such that

$$\frac{C_V(z=0)}{C_V(z=L_z)} = \xi. \tag{6.1}$$

At $z = L_z/2$, the vacancy concentration is kept at C_V^0. Thus the distribution along z-axis is given by

$$C_V(z) \quad = \quad (\frac{2C_V^0}{1+\xi})[\xi + (1-\xi)\frac{z}{L_z}]. \tag{6.2}$$

Secondly, during the diffusion simulations, if a lattice-continuation (in Chapter 4) happens to a migrating vacancy, the total binding energy Eq.(4.1) will include the change as

$$\Delta E_i \quad = \quad (n_{1nn}\Delta E_{1nn} + n_{2nn}\Delta E_{2nn} + n_{3nn}\Delta E_{3nn}) \pm \frac{kT}{2}\log(\xi), \tag{6.3}$$

where $\pm$ stands for the edge of $z = L_z$ or $z = 0$. If a vacancy migrates forwards on the z-axis, by jumping from $z < L_z$ to $z > 0$, the positive sign is taken in Eq. (6.3). If a vacancy migrates in the reverse direction, the negative sign is taken in Eq. (6.3). The records of the vacancy distribution exhibit a well maintained vacancy gradient throughout the diffusion simulations as shown in Figure 6.1.

From Figure 6.1, the number of vacancies on each XY plane appears quite stable despite substantial deviations from linearity. Throughout the system, dopant atoms are randomly distributed. Compared to the motion of vacancy, dopant atoms

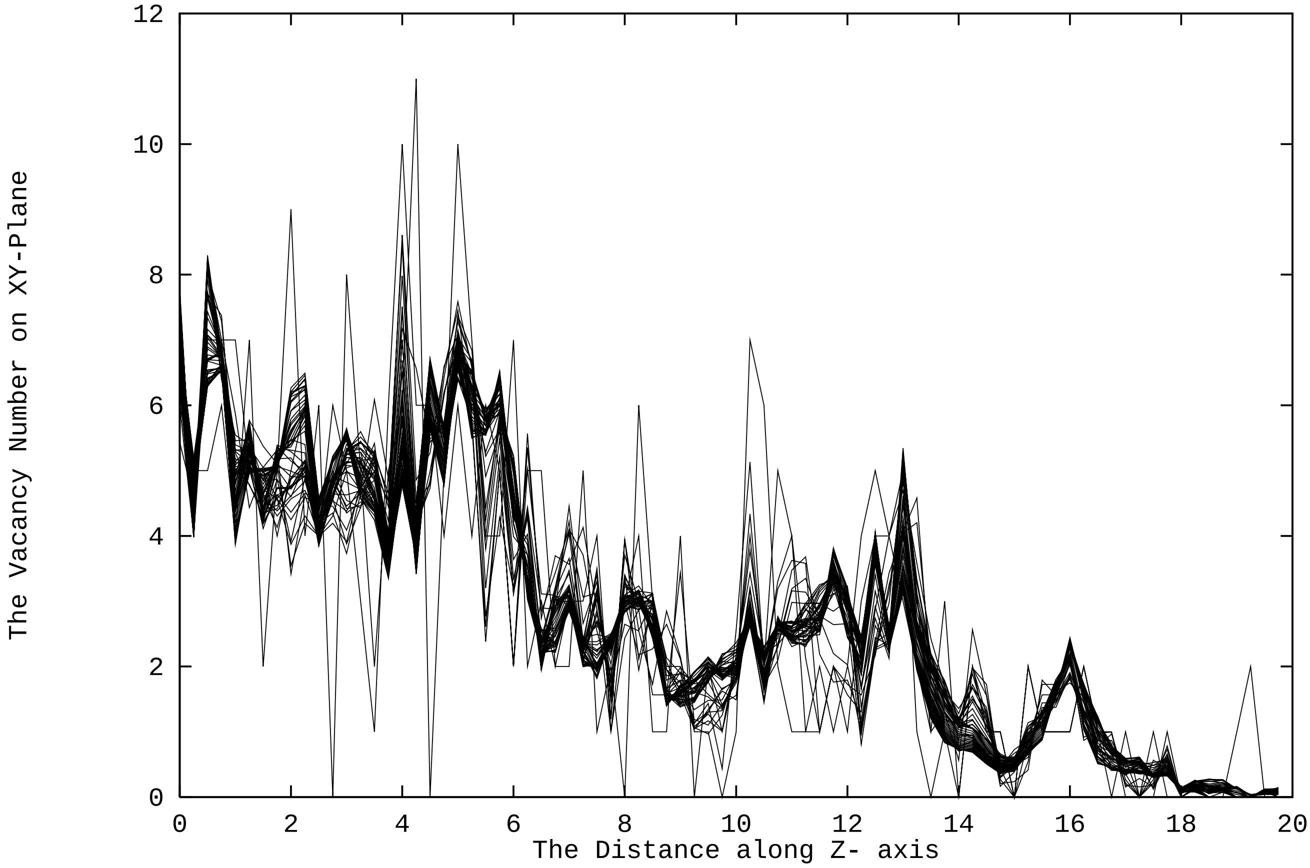

Figure 6.1: The vacancy distribution along z-axis with $C_V(z=0) = 20C_V(z=L_z)$ and lattice size $20 \times 120 \times 120$, where the data are taken every 200K steps from a Monte Carlo random walk simulations with 5 million steps.

change their sites much less frequently once decided by the initial distribution. The highest vacancy occupation is for the sites near dopant atoms. Thus we expect for that throughout the diffusion process, vacancies are most likely on the XY planes with the highest doping densities.

6.2 Vacancy Gradient Effect on Dopant Flux

Based on dopant-vacancy pair diffusion theory [1], with a vacancy gradient along the z-axis, the resulting flux of dopant atoms is given by

$$J_D^V = -D_{DV}\frac{\partial}{\partial z}C_{DV}, \tag{6.4}$$

where D_{DV} is the diffusivity of dopant/vacancy pair and C_{DV} is the pair concentration. Using Eq.(2.3), we have

$$J_D^V = -D_{DV}K_{D/V}\left(C_V\frac{\partial C_D}{\partial z} + C_D\frac{\partial C_V}{\partial z}\right), \tag{6.5}$$

where $K_{D/V}$ is the pairing coefficient. As measured by the simulations in Chapter 4 and 5, the effective diffusivity can be written as

$$D_D = D_{DV}K_{D/V}C_V^0, \tag{6.6}$$

where C_V^0 is the free vacancy concentration. If the vacancies are uniformly distributed, $J_D^V = 0$ as we have confirmed from simulations presented in Chapter 4 and 5. However, in the presence of a vacancy gradient, we have the dopant flux of

$$J_D^V = -\frac{D_D C_D}{C_V^0}\left(\frac{\partial C_V}{\partial z}\right), \tag{6.7}$$

where the effective dopant diffusivity D_D is as calculated from Eq. (3.13).

The pair diffusion model is an idealized model for vacancy-mediated diffusion, which supposes that dopant and vacancy are tightly bound and diffuse as a pair. However, from the vacancy mechanism, the dopant could have long-range migration only after vacancy move away from the dopant atom at least the $3nn$ site distance. This means that the migration of vacancy is not necessarily coincident with the migration of dopant atom. Depending on the interaction potential, dopant-vacancy pairs can dissociate during the diffusion process, leading to a weaker dependence of the dopant flux on the vacancy gradient. Thus, the flux equation could be modified as

$$J_D = -\frac{D_D}{C_V^0}(C_V\frac{\partial C_D}{\partial z} + \gamma C_D\frac{\partial C_V}{\partial z}), \tag{6.8}$$

where γ is a measure of vacancy contribution to the dopant flux. If $\gamma = 1$, the equation is for the dopant-vacancy pair flux J_D^V. If $\gamma = -2$, which is used by Maser

[14], the dopant flux is in the opposite direction to the vacancy flux. As an extreme example of $\gamma = -2$, for vacancy-mediated self-diffusion, the silicon flux J_{Si}^{V} is equal and opposite to the vacancy flux as each vacancy hop displaces a silicon atom in the opposite direction.

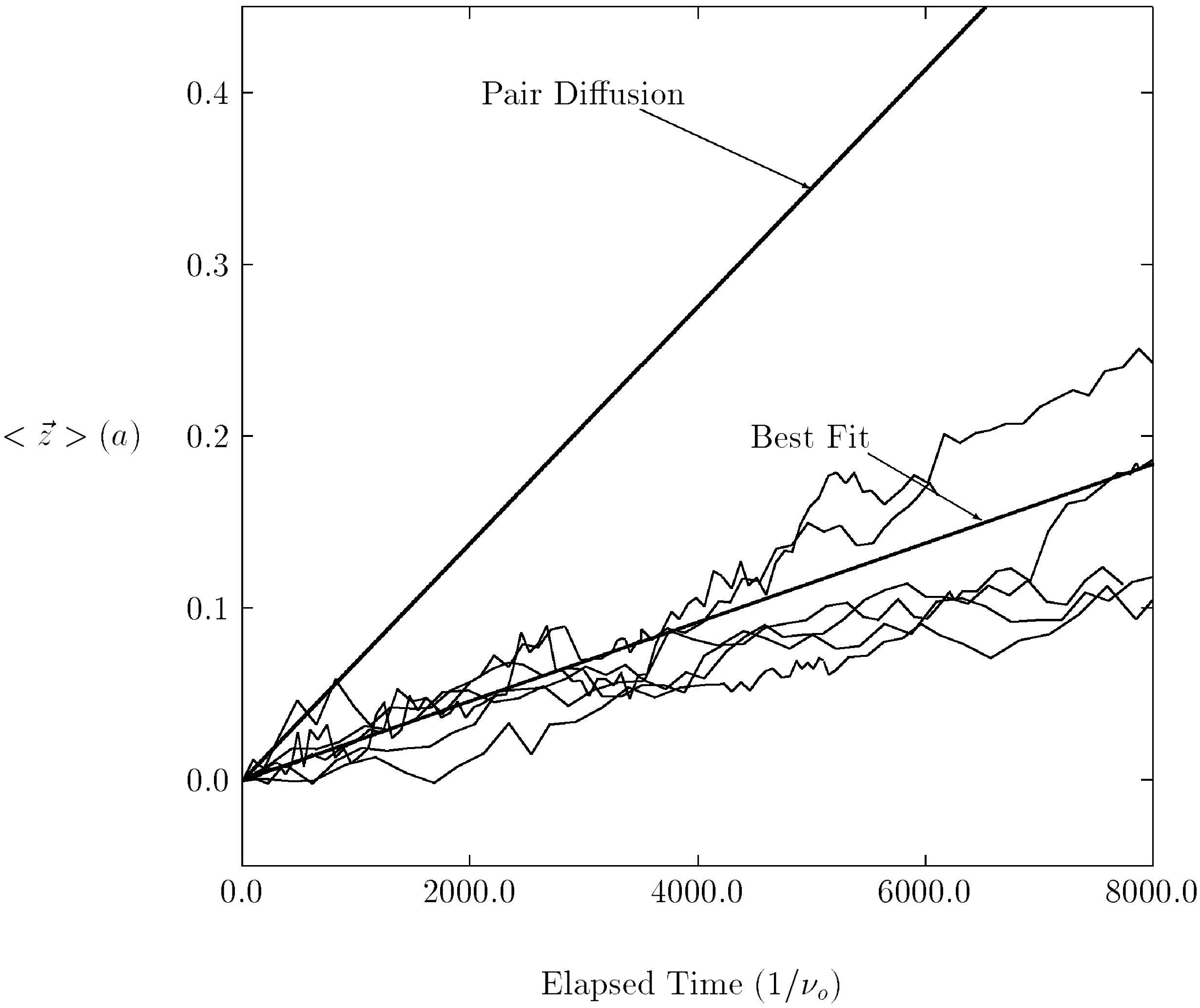

Figure 6.2: The total elapsed time versus the average displacement of dopant atoms along z-direction in unit of lattice constant a, where the pair diffusion line indicates pair diffusion model of J_D^V and the best fit line is for a modified flux equation fitted to the simulation results.

Now, we are going to discuss our simulation results on this topic. The simulations utilize a lattice with $N_z \times N_x \times N_y = 10 \times 120 \times 120$ with a difference of vacancy concentration applied to two edges along the z-axis as

$$\frac{C_V(z=0)}{C_V(z=L_z)} = \xi \simeq 7.4, \tag{6.9}$$

where $L_z = N_z \times a$ (a is lattice constant). The dopant/vacancy pair binding energies are $E\{12kT, 8kT, 4kT\}$ with fixed dopant density $C_D = 1.5 \times 10^{19}\text{cm}^{-3}$ and average free vacancy concentration $\langle C_V^0 \rangle = C_V(z = L_z/2) = 5 \times 10^{16}\text{cm}^{-3}$. The average displacement per time of dopant atoms along the Z-axis, which is related to the flux, was calculated by

$$\frac{<\vec{z}>}{t} = \frac{J_D}{C_D}. \tag{6.10}$$

With the modified dopant flux equation, I get the formula for dopant displacement rate caused by the vacancy gradient as

$$\begin{aligned} \frac{<\vec{z}>}{t} &= -\gamma(\frac{2D_D}{L_z})[\frac{1-\xi}{1+\xi}] \\ &= 6.9 \times 10^{-5}\gamma(\frac{a}{\nu_o}) \end{aligned} \tag{6.11}$$

where the displacement is in the unit of lattice cell length a, the elapsed time is in unit of $1/\nu_o$ (ν_o is the vacancy hopping rate in self-diffusion) and the diffusivity formula of Eq.(3.13) is used.

Our simulation results in Fig.6.2 suggest that the best fit curve for the flux equation Eq.(6.8) should have $\gamma \simeq 1/3$. With $\gamma = 1/3$, we can confirm that with the binding energies corresponding to arsenic at 915^oC, the dopant flux has the same direction as the vacancy flux, which is qualitatively consistent with predictions based on pair diffusion theories [13]. However, in the diffusion process, $\gamma < 1$ indicating that the dopant/vacancy pairs do not always remain tightly bound.

List *et al.* [15, 38] used the attractive potential well of

$$\begin{aligned} &\mid \Delta E_0 \mid = ... = \mid \Delta E_i \mid = 4kT, \\ &\mid \Delta E_{i+1} \mid = ... = \mid \Delta E_\infty \mid = 0; \end{aligned} \tag{6.12}$$

where i represents the ith-nearest neighbor site and $i = 0, 1, 2, 3$ was used by List *et al.*. They obtained γ from

$$\gamma = \frac{T_D^0}{D_D^0}, \tag{6.13}$$

where D_D^0 in intrinsic dopant diffusivity and T_D^0 is a dopant transport coefficient which is related to the pair interaction potentials, via jump frequency calculations.

The results by List *et al.* show that for tracer diffusion ($i = 0$), $\gamma = -1.92$ and with the potential well, out to the $1nn$ site ($i = 1$) $\gamma = -1.83$; out to the $2nn$ site ($i = 2$), $\gamma = -1.52$; and out to the $3nn$ site, $\gamma = 0.55$. Since in our research, we use a potential out the $3nn$ site distance, our results of $\gamma = 1/3$ are consistent with the results of List *et al.* Our simulations and List's results suggest that γ is dependent on the types and ranges of pair binding energy, but that a value less than one is appropriate for dopants in silicon.

If we change the values of pair binding energies, we can expect a different γ. As the binding energies are increased, the dopant-vacancy pair are more tightly bound, the γ should be increased. The γ will become less than $1/3$ if we reduce the binding energies. If the doping density is increased to a high value so that the dopant number is much larger than vacancy number, γ could become negative, since the dopant flux may have an opposite direction against the vacancy flux. The extreme example is of silicon flux (self-diffusion) in a vacancy gradient.

Chapter 7

Conclusions and Suggestions for Future Work

In this research, a Monte Carlo simulation program was designed to trace the motions of dopants and vacancies through the microstructure of the three-dimensional silicon lattice. With the computational simulations, we have investigated not only how the diffusivity depends on the dopant density and vacancy concentration, but also how diffusion behavior is related to the binding energies of the dopant-vacancy pair. The simulation results have demonstrated the new atomistic model of vacancy-mediated diffusion as a more accurate model than Hu's model [1, 6, 17], by defining the diffusivity as a function of the dopant-vacancy interaction energies with different pair distances.

In the simulations of vacancy-mediated diffusion, we find that when the doping density is moderate, the diffusivity is decided by the vacancy concentration and the binding energies between the dopant atom and vacancies with the 2nd-nearest and 3rd-nearest neighbor distances. After doping density increases above a certain critical value ($\sim 2.0 \times 10^{20}\text{cm}^{-3}$), the diffusivity changes from the linear function typical of Fermi level effects to cubic or quartic or even higher order power functions of the doping density as predicted by the atomistic model. The simulation results have shown a great consistency with the experimental results obtained by previous researchers [10, 28, 29].

An investigation was also done on dopant fluxes caused by a vacancy gradient. The Monte Carlo simulation program was developed to maintain a vacancy gradient during the process of dopant diffusion. The average displacement of dopant atoms was derived as a linear function of the elapsed time to match the simulation results. It was demonstrated that both the dopant flux and vacancy flux have the same direction in the gradient of vacancy concentration, but the binding of the dopant-vacancy pair is weaker than the assumption from pair diffusion model, leading to a modification of the coupled diffusion equations.

As to suggestions for further work on this subject, the Monte Carlo simulation can be improved to not only consider the dopant-vacancy pair interactions within the third-nearest neighbor distance, but also to extend the interactions to the fourth- or the fifth-nearest neighbor sites and to a broader range of variation in interaction potentials with distance.

Regarding the dopant flux caused by vacancy gradient, further simulations could investigate how the increasing the doping density and/or changing the binding energies affects the dopant flux.

So far, the binding energies used in my research have been qualitatively evaluated. For the Monte Carlo diffusion simulations in the future, it may be possible to have the pair binding energies precisely calculated as a function of dopant-vacancy site distance by recently developed techniques of *ab initio* total-energy calculations [34, 39, 40].

Finally, to make the simulation more complete, dopant-interstitial interactions should be considered in addition to the dopant-vacancy pair interactions.

Bibliography

[1] P. M. Fahey, P. B. Griffin and J. D. Plummer, *Reviews of Modern Physics* **61**, No. 2, 289 (1989).

[2] S. M. Hu, *Phys. Rev.* **180**, 773 (1969).

[3] M. Yoshida, E. Arai, H. Nakamura and Y. Terunuma, *J. Appl. Phys.* **45**, 1498 (1974).

[4] D. Mathiot and J. C. Pfister, *Appl. Phys. Lett.* **47**(9), 962 (1985).

[5] S. T. Dunham, *J. Electrochem. Soc.* **139**, No.9, 2628 (1992).

[6] S. M. Hu, *J. Appl. Phys.* **45**, 1567 (1974).

[7] D. Mathiot and J. C. Pfister, *J. Physique Letters* **43**, L-453 (1982).

[8] D. Mathiot and J. C. Pfister, *J. Appl. Phys.* , **55**, 3518 (1984).

[9] D. Mathiot and J. C. Pfister, *J. Appl. Phys.*, **66**, 970 (1989).

[10] A. Nylandsted Larsen, K. K. Larsen, P. E. Andersen and B. G. Svensson, *J. Appl. Phys.* **73**(2), 691 (1993).

[11] F. F. Morehead and R. F. Lever, *J. Appl. Phys.* **66**, 5349 (1989).

[12] B. J. Mulvaney and W. B. Richardson, *Appl. Phys. Lett* **51**, 1439 (1987).

[13] M. Orlowsky, *Appl. Phys. Lett.* **53**, 1323 (1988).

[14] K. Maser, *Experimentelle Technik der Physik* **39**, 169 (1991).

[15] S. List, P. Pichler and H. Ryssel, *SISDEP*, 1 (1993).

[16] S. M. Hu and S. Schmidt, *J. Appl. Phys.* **39**, 4272 (1968).

[17] S. M. Hu, *Phys. Status. Solidi* **B60**, 595 (1973).

[18] R. B. Fair, in *Impurity Doping Processes in Silicon*, edited by F.F.Y.Wang, 317-442 (North-Holland, Amsterdam, 1981).

[19] M. D. Giles, *IEEE Trans. Computer-Aided Design* **8**, 460 (1989).

[20] G. D. Watkins, *Inst. Phys. Conf. Ser.* No.**23**, 1 (1975).

[21] K. Compaan and Y. Haven, *Trans. Faraday Soc.* **54**, 1498, (1956).

[22] S. T. Dunham and C. D. Wu, *IEEE NUPAD* **V**, 101 (1994).

[23] S. T. Dunham and C. D. Wu, *J. Appl. Phys.*, in reviewed.

[24] A. D. LeClaire and A. B. Lidiard, *Philos. Mag.* **1**, 518 (1956).

[25] M. Yoshida, *J. Appl. Phys.* **48**, 2169 (1977).

[26] R. B. Fair, M. L. Manda and J. J. Wortman, *J. Mater. Res.*, **1** No.5, 705 (1986).

[27] F. Wittel and S. T. Dunham, *Appl. Phys. Lett.*, in press.

[28] A. Nylandsted Larsen, S. Yu. Shiryaev. E. Schwartz. Sorensen, and P. Tidemand-Petersson, *Appl. Phys. Lett.* **48**, 1805 (1986).

[29] P. E. Andersen, A. Nylandsted Larsen, P. Tidemand-Petersson and G. Weyer, *Appl. Phys. Lett.* **53**, 29 (1988).

[30] P. A. Flinn and G. M. McManus, *Phys. Rev.* **124**, 54 (1961).

[31] C. H. Bennett, *"Diffusion in Solids: Recent Developments"*, (A.S.Nowick and J.J.Burton eds.) p.73, Academic Press, New York (1975).

[32] G. E. Murch, in *Diffusion in Crystalline Solids*, edited by G.E.Murch and A.S.Nowick, 379-427 (Academic Press, 1984).

[33] G. Jacucci, in *Diffusion in Crystalline Solids*, edited by G. E. Murch and A. S. Nowick, 429-482 (Academic Press, 1984).

[34] Y. Bar-Yam and J. D. Joannopoulos, *Phys. Rev. Lett.* **52**, 1129 (1984).

[35] M. Hirata, M. Hirata and H. Saito, *J. Phys. Soc. Jpn.* **27**, 405 (1969).

[36] S. Chandrasekhar, *Rev. Mod. Phys.* **15**, 1 (1943).

[37] H. Bracht, N. A. Stolwijk, I. Yonenaga, and H. Meherer, *Phys. Stat. Sol.* **137**, 499 (1994).

[38] S. List, P. Pichler and H. Ryssel *In Press* (1994).

[39] Y. Bar-Yam, S. T. Pantelides and J. D. Joannopoulos, *Phys. Rev.*, B**39**, 3396 (1989).

[40] M. C. Payne, M. P. Teter, D. C. Allen, T. A. Arias and J. D. Joannopoulos, *Rev. Mod. Phys.*, **64**, No.4, 1045 (1992).